We are IntechOpen,
the world's leading publisher of
Open Access books
Built by scientists, for scientists

4,800
Open access books available

122,000
International authors and editors

135M
Downloads

Our authors are among the

154
Countries delivered to

TOP 1%
most cited scientists

12.2%
Contributors from top 500 universities

CLARIVATE ANALYTICS
BOOK CITATION INDEX
INDEXED

WEB OF SCIENCE™

Selection of our books indexed in the Book Citation Index
in Web of Science™ Core Collection (BKCI)

Interested in publishing with us?
Contact book.department@intechopen.com

Numbers displayed above are based on latest data collected.
For more information visit www.intechopen.com

Prospective Monte Carlo Simulation for Choosing High Efficient Detectors for Small-Field Dosimetry

Hossam Donya, Baljeet Seniwal, Reem Darwesh and Telma C.F. Fonseca

Abstract

In this chapter, a detailed study on physics and methodology of small field dosimetry are reported. It introduces talking about how small radiation fields came into existence and the importance of accurate small-field dosimetry. In addition, it discusses small and long cavity theories for evaluating accurate dose response. It sheds the spot on pencil beam algorithms for evaluating dose response and uses Monte Carlo (MC) simulation in categorizing primary and scattering components of the radiotherapeutic photon beam. Moreover, it summarizes all commercial dosimeters used in small-field dosimetry. It gives good knowledge about detectors and equipment like ionization chambers for reference dosimetry in small and non-reference fields and different types of solid-state detector. The importance and applications of Monte Carlo techniques in small-field dosimetry and radio-therapeutic treatment methods based on small field are reported. For this purpose, different commonly used Monte Carlo codes are handled like Electron Gamma Shower (EGSnrc), Geant4, PENELOPE, and Monte Carlo N-Particle (MCNP). A review on the recent studies of using Monte Carlo simulation particularly on the small-field dosimetric studies is also reported. This chapter also discusses the recommendations of the code of practices (COPs) for dosimetry of small radiation fields. It mentions all recommendations provided by TRS-483 for accurate beam data collection and accurate dosimetric measurements. It gives good knowledge to the user for selecting a suitable dosimeter in small-field dosimetry through investigation of different practical methods and Monte Carlo simulations.

Keywords: Monte Carlo simulation, radiotherapy physics, small-field dosimetry, machine-specific reference field, cavity theory, output factors

1. Introduction

In the current state of external photon beam radiation therapy, the "small fields" are generated by collimating the photon beam, flattened or unflattened. This is done with the help of collimating system available on medical electron linear accelerators (linacs), which includes secondary jaws, multi-leaf collimators (MLCs), tertiary collimators, etc. [1]. The small photon beams differ from traditionally used

radiation fields (4 cm × 4 cm up to 40 cm × 40 cm) in terms of their size. Due to their small size, the penumbra region generated from the edges of the fields overlap, resulting in apparent field widening of the fields [2]. As a result the traditional detectors used for dosimetry become large relative to the size of the field, and this may lead to unintended errors while performing measurements for small field [3].

The widely accepted Code of Practices (COPs) reported in the Technical Reports Series No.398 of IAEA have procedures to determine absorbed dose to water from measurements made with an ionization chamber in photon, electron, proton, and heavy-ion beams [4–7]. The ionization chambers are used to perform the measurement using the calibration coefficients obtained from primary standard dosimetry laboratories (PSDL) in terms of absorbed dose to water under reference conditions. However, these COPs do not consider the conditions deviating from reference conditions in detail [8].

As a result of technological improvements and introduction to new radiation therapy techniques, the small static radiation beams are rapidly used, which is achieved by using standard or add-on MLCs or by the design of the radiation equipment. Consequently, the uncertainties related to the clinical dosimetry based on traditionally used COPs have been considerably increasing, and errors related to dosimetry have been growing larger. The main causes of this increase in the size of dosimetric errors are that it is not possible to achieve the reference conditions as recommended by traditional COPs on some radiation equipment and non-standardization of dose measurement procedures in small and composite radiation fields. Hence, many accidents have been reported that have occurred due to the use of recommendations of traditional COPs in dosimetry of small fields [8, 9].

The dosimetry of small fields is quite important. The beam data once configured during commissioning will be used for treatment in the future, so there should be high accuracy in the dosimetry of these small fields. To achieve high accuracy in beam data measurement in small fields and to be able to measure the dose in small fields with high precision, it is quite important to understand the physical aspects of the small fields. The measurement of output factors, beam profiles, and depth dose data is highly influenced by the beam energy, scattering, and field dimensions at the level of detector. The knowledge of the important characteristics of small fields is required to measure the dose parameters and to collect data for treatment. Hence, in 2017 a joint working group from the International Atomic Energy Agency (IAEA) and American Association of Physicists in Medicine (AAPM) proposed a new COP, Technical Report Series (TRS) No. 483 (Dosimetry of Small Static Fields Used in External Beam Radiotherapy). [9] This COP provides recommendations related to the relative and reference dosimetry of small and composite fields. Hence, this chapter discusses the concepts related to the dosimetry of small and composite field sizes.

2. Field size definition

In general, two types of field sizes have been defined by the International Electrotechnical Commission. The first is called the *geometric field size*; it is defined as two-dimensional projection by the source of radiation of the collimator opening on a plane orthogonal to the central axis of the primary photon beam. The second is called the *irradiation field size*; it is defined as the two-dimensional area bounded by specific isodose lines in a plane orthogonal to the central axis of the radiation beam. An alternative way to define irradiation field size is by using full width at half maximum (FWHM) of radiation beam profiles obtained along the lateral direction (in-line or crossline profiles) at isocenter depth. This FWHM is equal to the opening of the collimating jaws at the isocenter. Therefore, at isocenter the geometrical and irradiation fields are in consonance with each other. Hence, this agreement can be

verified by FWHM measurement of the beam profile along the lateral direction. However, in the small beam condition due to the partial blockage of primary source of photon and reduction in the head scatter along the central axis, the output of radiation is reduced. As a consequence the condition of lateral charged particle equilibrium (LCPE) is not fulfilled. Hence, due to the reduction in the radiation output along the central axis, the value of maximum dose also gets reduced, and agreement between the geometrical and irradiation fields is lost. **Figure 1** illustrates the overlapping of penumbra region with decrease in field size, as it leads to decrease in output and increase in penumbra width. Hence, the parameters like FWHM breaks down for small-field sizes [3, 10]. In case of small beams due to the overlap of penumbra region, the FWHM of the profile gets broader relative to the collimator settings, and this effect is called apparent field widening.

2.1 Conditions of small beam

2.1.1 Definition of small field

Any radiation beam which fulfills at least one of the following conditions can be named as small field:

    i. The absence of LCPE along the central axis of the radiation field (see **Figure 1**).

    ii. The partial blockage of the radiation source by the collimating devices along the central axis (see **Figure 2**).

    iii. The detector size is equal to or larger than the size of the radiation beam (see **Figure 3**).

Conditions I and II are related to the size of the radiation beam, whereas condition III refers to the size of the detector. If all the above mentioned conditions are fulfilled, then the penumbra region overlaps with the volume of the detector.
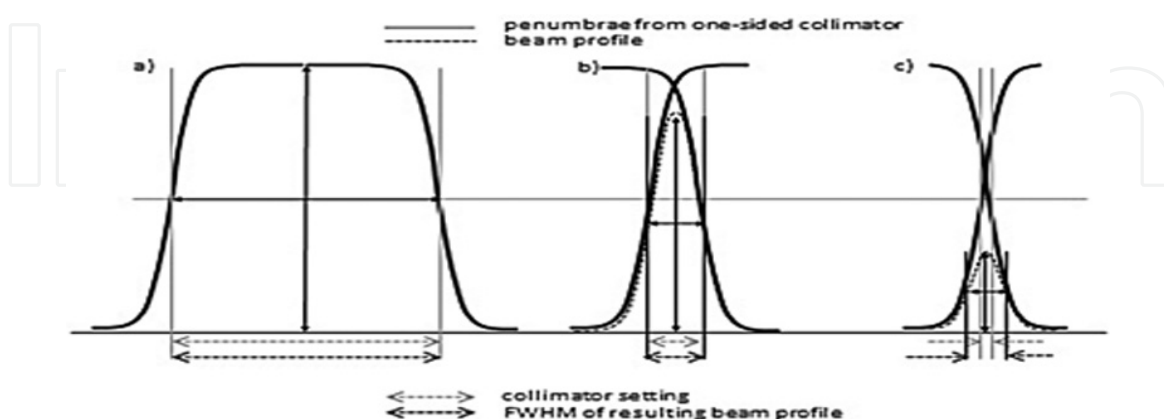
Figure 1.
Schematic illustration of the definition of geometrical and irradiation field size using the concept of geometrical projection and FWHM of radiation beam profile for both broad and small beam conditions: (a) for large field sizes, where condition of LCPE is fulfilled and radiation source is not blocked, the full width at half maximum (FWHM) of the lateral dose profiles is equal to the opening of the collimating jaws at the isocenter. Hence, for large field sizes at isocenter, geometrical field size and irradiation field size are in agreement with each other; (b) for the field sizes of the order of the range of secondary charged particles, the penumbra region of opposite jaws. It results in small error in determining the field size from the FWHM of lateral beam profiles; (c) however, for small field sizes due to the reduction in the radiation output along the central axis, the value of maximum dose is reduced. Hence, the FWHM of lateral beam profile is pushed outward and agreement between the geometrical and irradiation fields is lost.
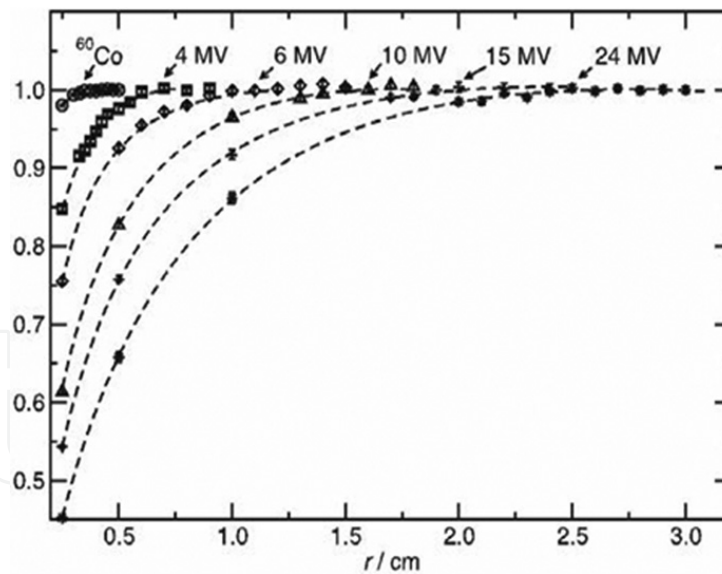
Figure 2.
The ratio of collisional kerma in water and absorbed dose in water at a depth of 5 cm. Source to surface distance (SSD) of 80 cm is used for Co⁶⁰ and SSD of 100 cm was used for photon beam. X axis represents the radius of the beam and the Y axis represents the ratio of the quantities.

2.1.1.1 Conditions based on field size

For the radiation beams with FWHM lesser than the maximum range of the secondary electrons, the LCPE is absent. The absence of LCPE makes it difficult to perform measurements for absorbed dose to water for detectors made of non-water equivalent material. In order to find a relation between the size of the beam and the size of the detector for which the LCPE exists, LCPE range (r_{LCPE}) has been proposed. r_{LCPE} can be defined as the minimum radius of circular photon field for which the ratio of collisional kerma in water and dose deposited in water is equal to 1 at the center of the beam. **Figure 2** illustrates the concept of LCPE, where the ratio of collisional kerma in water and dose deposited in water are calculated using Monte Carlo simulations at a depth of 5 cm along the central axis of the radiation beam [11].

r_{LCPE} (in cm) can be manifested as a function of beam quality of photon beam, Tissue Phantom Ratio (TPR), $TPR_{20,10}(10)$:

$$r_{LCPE} = 8.369 \times TPR_{20,10}(10) - 4.382 \qquad (1)$$

In the case of beam quality defined in terms of percentage depth dose at a depth of 10 cm, $\%dd(10,10)_x$, r_{LCPE} can be calculated using the correspondence between $\%dd(10,10)_x$ and $TPR_{20,10}(10)$ [12]:

$$r_{LCPE} = 77.97 \times 10^{-3} \times \%dd(10,10)_x - 4.382 \qquad (2)$$

The second condition related to the partial blockage of the primary radiation source is illustrated in **Figure 3**. It is based on the finite size of the extended focal spot, which can be determined by FWHM measurement of bremsstrahlung spectrum emitted by the radiation source. The partial shielding of the radiation source by the beam modifier, used for the definition of small beam, results in decrement of radiation output along the central axis of the radiation beam relative to the unshielded condition. The radiation beams with size equal to or less than the FWHM of the emission spectra emitted from the source, the effect of partial occlusion of radiation source becomes more dominant. Since the source size is generally

less than 5 mm, as it can be observed from **Figure 2**, the loss of LCPE also starts for radiation beams with a radius of 5 mm. Therefore, the partial blockage of radiation source starts when loss of charge equilibrium starts [1]. The partial blockage of radiation source results in a decrease in the beam output. Hence, result in the sharp dose gradient, as a consequence of which the response of the detector is affected.

Therefore, the absence of LCPE and partial blockage of small beams of photon radiation source is the main cause of the decrease in the radiation output along the beam axis. This effect gets more dominant with increase in the energy of the radiation beam and decrease in the density of the medium.

2.1.1.2 Conditions related to detector size

The last condition is related to the size of the detector relative to the size of the radiation beam. The signal produced by the detector on irradiation is directly proportional to the average of the deposited dose within the detector's sensitive volume. The signal obtained from the detector is responsive to the uniformity of deposited radiation dose over the sensitive volume of the detector, also known as volume averaging as illustrated in **Figure 4** [13]. Hence, in order to obtain dose
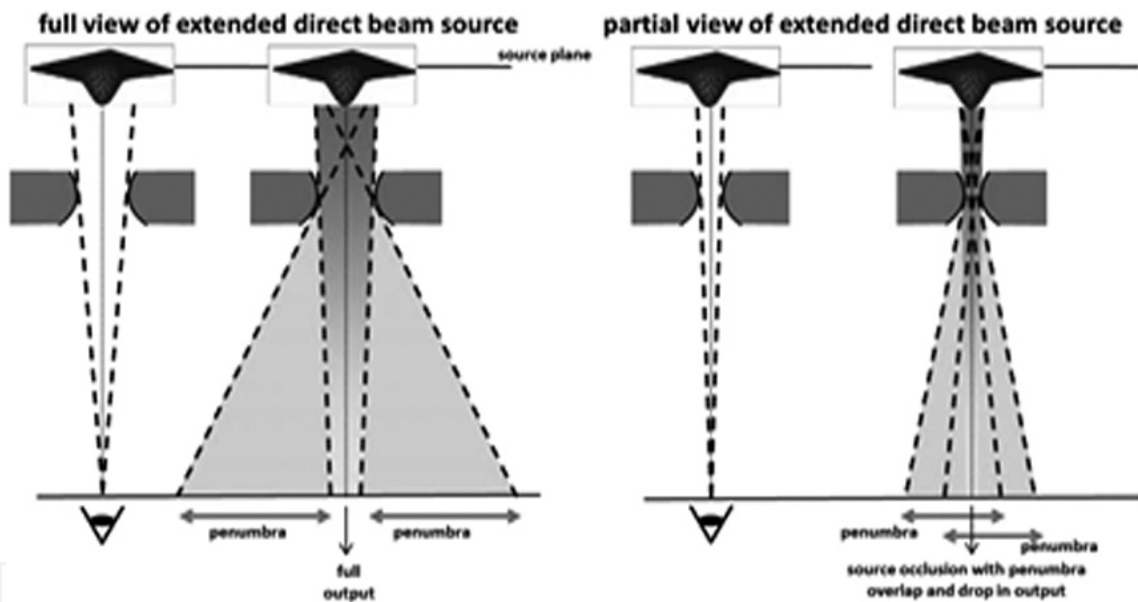
Figure 3.
A schematic illustration of the source occlusion effect.
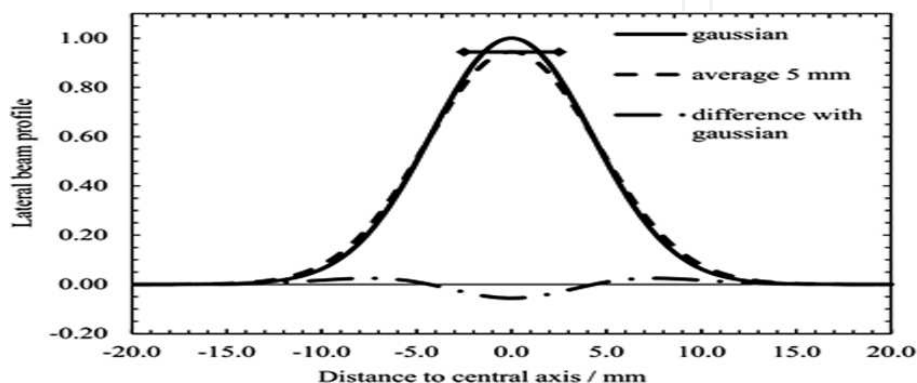
Figure 4.
A schematic representation of volume averaging effect along the central axis of the beam. The Gaussian curve in black represents the actual beam profile; the measured profile obtained using the detector (5 mm long) is given represented by dashed line; the dimensions of the detector along the scanning axis is represented by double arrow; the variation between the measured profile and Gaussian curve is given by dash-dotted line.

deposited to the water from the signal produced by the detector, the correction factor must be used for the volume averaging. It can be defined as a ratio of dose deposited in water at the point of reference in the nonexistence of the detector to the average of the dose deposited over the detection volume of the detector in the nonexistence of the detector. It can be acquired by integrating the three-dimensional distribution of dose over the detector's sensitive volume [14–19].

The general expression that can be used in calculation of correction factor for averaging of the signal over the detector's sensitive volume is:

$$k_{vol} = \frac{\iint_A w(x, y)\, dxdy}{\iint_A w(x, y)\, OAR(x, y)\, dxdy} \tag{3}$$

where (x,y) are the positions of the points on the axis orthogonal to the beam axis, A is the projected area of the detector's sensitive volume in a plane perpendicular to the central axis of the beam, OAR (x,y) gives the off-axis ratio at position (x,y), and w(x) is the weighting function that represents extension of cavity of the air-filled detector along the central axis (z) of the beam in relation to the lateral coordinates of the beam (x and y).

The volume averaging effect and the disturbance caused by the existence of detector to the fluence of the charged particles are two main effects observed in small beam dose measurement. As discussed above, due to the presence of dose gradients and absence of LCPE, the perturbation effect becomes dominant and cannot be modeled easily. Along with this, the errors related to the averaging of the detector signal along its volume become larger. Consequently, the dose gradients and nonexistence of LCPE make it difficult to perform dosimetric measurements for small beams.

The radiation fields, having the distance between the edges of the field and outer surface of the detector volume less than the r_{LCPE} within a medium, satisfy the small beam condition. In order to prevent such condition and perform dosimetric measurements accurately, the FWHM or the radius of the photon beam must be equal to the sum of r_{LCPE} and half of the detector's outer volume.

2.2 The machine-specific reference field (f_{msr})

For radiotherapy radiation emitters, where the reference beam size (f_{ref}) of 10 cm × 10 cm cannot be obtained, a new concept of machine-specific reference (msr) field size has been proposed. The dimensions of the msr field (f_{msr}) should be as close as possible to that of f_{ref} and must be at least equal to the sum of r_{LCPE} and half of the detector's outer volume.

3. Detectors and equipment

3.1 Ionization chambers for reference dosimetry in small and non-reference fields

An ideal air-filled detector to be used for measurement of dose deposited in water must be equivalent to the water and not perturb the charged particle fluence; its response must not be affected by dose rate or directional dependence; it must show good sensitivity, in terms of signal to noise ratio and time taken to obtain the

signal; the detector signal must be beam energy independent and directly proportional to the dose deposited in water; and it must show minimum fluctuations, leakage, and no effect of cable irradiation.

The detector size must be such that it fulfills r_{LCPE} criteria. The positioning of the air-filled detector must be such that the charged particle fluence remains approximately uniform over the sensitive volume of the detector.

3.1.1 The square equivalent msr field (f_{msr}) greater than 6 cm × 6 cm

Modern radiotherapy linear accelerators are available in two general models, that is, with flattening filter (WFF) and flattening filter free (FFF). For WFF radiation emitters, air-filled detectors with sensitive volume range between 0.3 and 1 cm^3, since these detectors are often water resistant and easy to use for in-phantom measurements have negligible leakage effect and good signal to noise ratio [20]. In the case of FFF radiation emitters, air-filled detectors with sensitive volume lying in the range of 0.1–0.3 cm^3 are preferred over the commonly used Farmer type air-filled detectors [21]. In case the Farmer type air-filled detectors is used in FFF beam, then the beam profiles must be corrected for their non-uniformity; the factor for correction can be 1.5% for FFF photon beam of 6 MV [22, 23].

3.1.2 The square equivalent msr field (f_{msr}) less than 6 cm × 6 cm

A comparative study was performed by Le Roy et al. [24] using 24 small volume air-filled detectors of 8 different types, to study the probability of their use in high-energy photon beams for reference dosimetry, with beam size ranging down to 2 cm × 2 cm. The authors reported that out of eight different types of air-filled detectors only three types of chambers were found suitable for small beam dosimetry, which includes CC04, CC01 models from IBA, and AISL from Exradin.

In case of very small circular msr fields as that of Gamma Knife machine having the diameter of the radiation beam 1.6 or 1.8 cm. It is found that these fields exhibit LCPE, r_{LCPE} was found to be 0.6 cm for ^{60}Co [25]. The chambers fulfilling the condition of r_{LCPE} in msr fields are suitable for use in these very small circular fields for reference dosimetry.

The air-filled detectors with sensitive volume less than 0.3 cm^3 and air cavity length of 7 mm are preferred for dosimetric measurements for f_{msr} less than 6 cm × 6 cm. The criteria used for selection of detector volume and air cavity length can be demonstrated by relating it with the size of the radiation beam and beam energy. The detector with air cavity of 7 mm satisfies r_{LCPE} condition for field sizes down to 4 cm in 10 MV beam, down to 3 cm in 6 MV beam, and down to 2 cm for Co^{60} radiation beam.

3.2 Different types of detectors for relative dosimetry in small radiation beams

The concept of relative dosimetry is based on the determination of various dosimetric beam parameters, such as measurement of dose distribution with depth along central axis of the beam, lateral beam profiles, etc. as a function of the size of the radiation beam and its shape. The choice of appropriate detector is based on the specific type of parameter being measured. Hence, two or more suitable detectors of different kinds can be used to perform the same measurement to be sure about the accuracy of measurements.

For the measurements of output factor, volume averaging effect, dependence on the: size of the radiation beam; beam energy; dose rate; equivalence to water and overall perturbation are the deciding factors to find the suitable detector for

measurements. However, in case of beam profile measurements, the detectors with high spatial resolution, direction-independent response, dose-rate independence, and suitable volume are preferred. Since the selection of detector with suitable volume makes it possible to measure penumbra region accurately, uniformity in directional response may result in accurate measurement of beam profiles; dose rate independence is also important for accurate measurement of beam profiles. Otherwise, correction factors are required for each of these effects for accurate measurement. As in the case of dose-rate dependence, correction factor needs to be applied in case of FFF beams, as these beams have high dose rate per pulse in the center of the beam in comparison to the edges. Otherwise it may lead to overestimation in the region of beam with high dose rate.

There is no ideal detector available for relative dosimetry of small beams. A number of detectors that can be used for relative dosimetry have been described in literature, and each of these detectors has been discussed briefly below:

- *Small air-vented ionization chambers*: These detectors are also known as minichambers or pinpoint chambers. The sensitive volume of these detectors ranges from 0.001 to 0.3 cm^3. These can be used for measurements in radiation beams with size down to 2 cm $\times$ 2 cm [24, 26]. These detectors are dose-rate independent and have uniform response in all directions and appropriate response for photons of low energy.

- *Micro-ionization chambers*: Also known as microchambers. The sensitive volume of these detectors ranges from 0.002 to 0.01 cm^3. These detectors have small volume averaging effect, and sensitivity is also reduced due to small sensitive volume.

- *Liquid ionization chambers* (*LICs*): These chambers are filled with dielectric liquids, which results in higher chamber signal per detector volume than air-filled ionization chambers, due to the higher density of liquid than air. The chambers are almost water equivalent; hence the chamber perturbation effect is reduced. However, the chambers are dose-rate dependent because of its large recombination effect.

- *Silicon diodes*: The sensitive volume of these detectors is less than 0.2 mm^3. These detectors exhibit angular dependency because of its construction and material composition and small volume averaging effect. The axis of symmetry of these detectors must be placed on the central axis of the beam. These detectors exhibit over-response in the case of low-energy photons due to the non-water equivalence. For small beam measurement, the use of unshielded diodes is preferred over the use of shielded diodes, and for field sizes below 1 cm, output correction factors are needed to be applied [26–30]. For very small beam size measurements, stereotactic diodes can be utilized. The sensitivity of these detectors depends on the accumulated dose, and they have limited lifetime. Therefore, time-to-time checking for constancy of relative response must be performed.

- *Diamond detectors*: These detectors exhibit high sensitivity, energy independence, and uniform response in all directions [31]. However, having dose-rate dependence and substantial pre-irradiation are required. The natural diamond detectors have been replaced by the artificial chemical vapor deposition (CVD) diamonds [32–34]. The bias voltage is not required for these detectors while using them for dosimetric measurements [35, 36]. However,

due to the difference in mass density relative to water, output correction factors are required when these detectors are used in field sizes below 1 cm [37].

• *Plastic and organic scintillators*: In these detectors light is produced in the scintillator when it is exposed to radiation. These detectors are almost energy independent, equivalent to water in terms of mass energy coefficient and electron density, and exhibit linear response for measurement of dose deposition in water [14, 19, 38–40]. Hence, these detectors can be directly used to determine the dose deposited. The corrections are needed to be applied for the production of Cerenkov light in optical fiber, which is used to transport the signals outside the treatment room. Different methods such as the use of hollow core fibers or the use of spectral filtration had been proposed to correct it [41]. Exradin W1 was found to be the only commercially available plastic scintillator.

• *Radiochromic film dosimetry*: Radiochromic films are the detectors with superior dimensional resolution. These are self-developing films and do not need chemical processing for development [42]. In case of high-energy photon beams, the radiochromic films are almost equivalent to tissue, resistant to water, and nearly energy independent [42, 43]. These films can be read with the help of suitable flatbed scanner. Before reading the films, it must be calibrated in terms of dose deposited in water, the spatial non-uniformity in the response of film must be carefully considered, and the response of the scanner and effect of orientation of film on the signal must be considered and should be corrected [44]. The radiochromic film can be used for measurements of lateral beam profiles, penumbra region, and field output factors.

• *Thermoluminescent dosimeters* (*TLDs*): TLDs are available in the form of powder, chips, microchips, rods, and ribbon. The most commonly used TLD material is LiF:Mg,Ti. In order to determine the dose deposited in water from the reading of thermoluminescence response, correction factors must be applied for non-linear relationship with the signal and dose deposited and also fading of the signal and energy correction. In order to accurately perform measurements in small beams of photon, careful handling and control of procedures are required to obtain measurement uncertainty within 2% or better [19].

• *Optically stimulated luminescence detectors* (*OSLDs*): The linearity in response, dependence on beam energy, and dependence on dose rate are similar to that of TLDs. OSLDs are generally composed of Al_2O_3:C and are available in the form of rods, chips, and nano-dots. The principle used in measurement of dose is similar to that of TLDs. In OSLD system, laser light is used to eject the energy trapped as luminescence. They can be used both as passive dosimeters and online readout system by connecting them with laser-based readout system and optical fiber.

• *Radiophotoluminescent* (*RPL*) *dosimeters*: These are solid-state dosimeters (SSD) based on the principle of radiophotoluminescence. They are accumulation type dosimeters and use silver activated phosphate glass for the measurement to absorbed dose. RPL dosimeters are generally available in the form of glass rods. When this silver-activated glass rod is exposed to radiation, it resulted in formation of stable luminescence centers in silver ions. They can be read using

the technique of pulsed ultraviolet laser excitation. RPL dosimeters exhibit linear response, flat energy response in the energy range of keV and MeV, good reproducibility, good spatial resolution, and negligible fading of signal [45, 46].

- *Alanine:* Its macroscopic interaction coefficients and density are close to that of water. The exhibit volume averaging effect because of its large size, low sensitivity, and high doses of radiation is needed to be delivered to obtain reproducibility of less than 0.5%.

3.3 Solid-state dosimeters and dose response compensation in external radiotherapy

This section shed light on describing the dosimetric response of solid-state dosimeters that are used for the dose measurement of external radiotherapy. Two approaches are presented for this purpose. The first approach, implementation of empirical method approach that considers the radiation beam, is separated into two components: primary and scattered beams. The spectral variation of radio-therapeutic beam is evaluated by their contribution in the dose to the medium that contains the region of interest. Solid-state dosimeters of high-density materials have an over-response issue that is commonly used in large and small fields. Hence, compensation factor should be calculated based on beam parameters such as energy, field size, depth, and other irradiation parameters. Dealing with over-response issue is not an easy task; however, it generates a significant improvement in accuracy in dose measurements over non-compensated measurements.

The second approach is to implement a compensation method based on a modified cavity theory. In this method, dose response of solid-state dosimeter is described considering the local spectrum and monoenergetic response. The local spectrum could be obtained by convolution method of pencil beam kernels using a pre-evaluated database that considers different separated types of particles according to their history of interaction (primary photon and electron and secondary photons and electrons). On the other hand, monoenergetic response of solid-state dosimeter could be calculated using the Monte Carlo simulation using different codes like PENELOPE [47, 48]. The accuracy of compensation methods should be evaluated by comparing simulated data with the corresponding measurements. This approach could be applied in situations where there is no lateral electron equilibrium compared to the previous method of compensation. Since the compensation accuracy depends on the local reconstructed spectrum, it is possible to implement this process in more complex irradiation conditions such as small fields. However, this method requires specific information such as the field size, beam quality, and detector position. Yet using two dosimeters whose materials in the sensitive volume are different can be instead used without considering beam information and enough to evaluate over-response correction.

3.3.1 The first approach: primer-released contribution separation

Cunningham [49] proposed a method for separation of primary beam component out of beam spectrum through dose calculation technique for irregular fields. He assumed that dosimeter placement does not introduce any local spectral disturbance in the volume of interest and the difference of dose response between solid-state dosimeter and water depends on the material difference and the ionization spectrum. The primary component of the spectrum photon beam is dependent on the design of the collimation system, for example, the primary collimator and flattening filter [50]. Accordingly, the difference between dosimetric response of

solid-state dosimeter and water is due to the primary component of the beam that remains almost invariant for the given beam quality and does not depend on the volume. On the other hand, the scattered component of the photon beam depends largely on the volume surrounding it; therefore, it depends on dosimeter depth, irradiated field size, etc. Hence, it is convenient to calculate the difference of the response caused by these two components separately and additively combine the two parts at the end of the calculation. To quantify the response rate provided by the primary and scattered components, a scattered factor (SF) could be introduced, defined as follows:

$$SF_w = \frac{D_w^{sc}}{D_w^{pr}} \quad (4)$$

$$SF_{SSD} = \frac{D_{SSD}^{sc}}{D_{SSD}^{pr}} \quad (5)$$

where D_w^{sc} and D_w^{pr} correspond to the dose contributions in water by primary and scattered components of photon beam, respectively. A scattered factor of solid-state dosimeter may be defined in the same manner, as shown in Eq. (5). The scattered factor is dependent on the field size and depth position of the dosimeter.

The total dose of water (D_w) or SSD (D_{SSD}) is the sum of the two components, primary and scattered. This can be expressed in terms of scatter factor as follows:

$$D_w = D_w^{pr}(1 + SF_w) \quad (6)$$

$$D_{SSD} = D_{SSD}^{pr}(1 + SF_{SSD}) \quad (7)$$

The response factor (RF) of SSD dose to water ratio is defined as:

$$RF_w^{SSD} = \frac{D_{SSD}}{D_w} \quad (8)$$

Therefore, the dose response of SSD could be corrected and applied to all SSD measurement by the evaluation of RF_w^{SSD} before the measurement implementation. Eq. (8) can also be expressed in terms of scattered factor, combining Eqs. (6) and (7):

$$RF_w^{SSD} = \frac{D_{SSD}^{pr}(1 + SF_{SSD})}{D_w^{pr}(1 + SF_w)} \quad (9)$$

In this way, expressing the response factor to fulfill the following objectives: The ratio between the primary dose of SSD to the dose of water (D_{SSD}^{pr}/D_w^{pr}) can be considered relatively stable, because once the charged-particle equilibrium (CPE) is established, the local spectra of the primary electrons and photons remain invariant which are independent of irradiation condition variations. Therefore, the RF_w^{SSD} variation is due to the difference of the scattered component of both water and SSD. As a result, RF_w^{SSD} depends on the determination of the primary dose ratios and scattered factors (SF_{SSD}, SF_w). However, it could not be easy to evaluate the primary and scattered doses separately in experiments, especially for high-energetic photons, because it needs massive buildup of material, which is necessary to achieve CPE to introduce significant attenuation and wide contribution [51]. Nevertheless, the response factor could be evaluated in a small field where CPE is still achieved. So in small-field dosimetry, the evaluated RF_w^{SSD} is close to the D_{SSD}^{pr}/D_w^{pr} since the main

primary contribution component is dominant. Rewriting Eq. (9) for the last condition of small-field irradiation as reference condition to the following equation:

$$RF_w^{SSD} = \frac{D_{SSD}^{ref}(1+\gamma_{SSD})}{D_w^{ref}(1+\gamma_w)} \tag{10}$$

where D_{SSD}^{ref}/D_w^{ref} is the dose–response factor of SSD to the water in the reference condition (small field). γ_{SSD} and γ_w are introduced instead of SF_{SSD} and SF_w in Eq. (9), respectively, and could be written as follows:

$$\gamma_{SSD} = \frac{D_{SSD}}{D_{SSD}^{ref}} - 1 \tag{11}$$

$$\gamma_w = \frac{D_w}{D_w^{ref}} - 1 \tag{12}$$

where D_{SSD} and D_w correspond to the dose response of SSD and water in an arbitrary requirement. Both factors are used to describe primary component variation with respect to the scattering component in the reference condition. To calculate the response factor by interpolation or extrapolation, measure both the dose in water by ionization chamber and in SSD to establish a response factor table. So in experimental measurement setup as illustrated in **Figure 5**, choosing small-field area to be a reference condition that avoids scattering component for dose response of SSD. PMMA sheets could be arranged around the solid-state dosimeter to establish homogenous tissue equivalent material. Mentioning that, at least 10 cm thickness of PMMA should be placed below the detector to create a homogeneous volume for the backscattered radiation. However, the measurement of the dose at a reference point in water phantom is established by ionization chamber. In small-field dosimetry beyond the buildup region, the relative difference of dose response between SSD and ionization chamber in water should be minimum, as low as possible as the result of the stability of primary component of radiation. Therefore, it is easy to explore the scattering factors in a large field. On the other hand, the
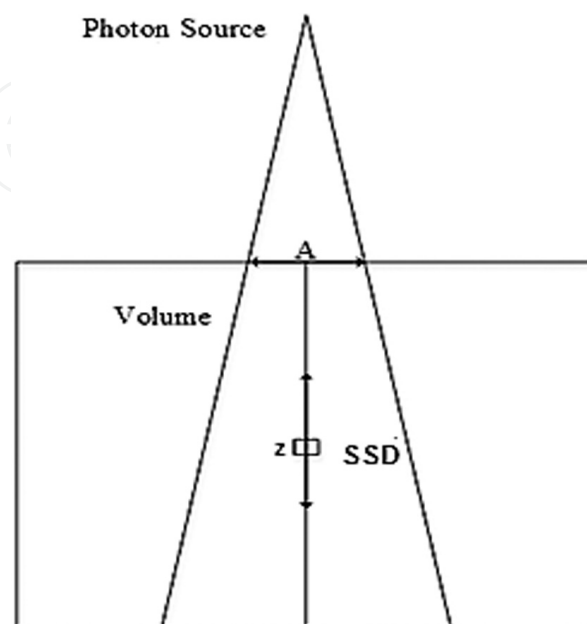
Figure 5.
Geometrical configuration.

spectral variation between SSD and ionization chamber is also affected by the depth of dosimeter. γ_{SSD} and γ_w could be evaluated from representing normalized maximum dose ratio or percentage depth dose for both dosimeters.

The relationship between γ_{SSD} and γ_w in small-field sizes may be linear due to the main contribution primary component. But the response factor linearity allows us to separate two sources that vary the local spectrum at the position of the detector: The size of the square field (A) and depth (z). Therefore, the response factor can be modeled by:

$$RF_{SSD} = 1 + k(z) \times (A - A_{ref}) \tag{13}$$

where the factor k(z) is a function of depth and A_{ref} corresponds to the size of the reference field (small-field size). Modeling of k(z) could be established from the slopes of plotted $RF_{SSD}(A)$ against the depth.

The previous characterization method of RF_{SSD} can be applied for a series of square field sizes with orthogonal collimators. However, in the case of irregular or circular fields, it must be expressed in terms of an equivalent square field for the interpolation. The method of equivalent square field is a simple empirical method for calculating the dose of irregular field size [52]. There are several ways to calculate the equivalent square field according to the literature: Equivalent tables for rectangular fields [53], sum of the small rectangles [54], and Clarkson integration of [55, 56]. Sterling's formula [57] can be used to calculate the equivalent square fields of the two rectangular fields:

$$ESQ = \frac{2WL}{(W + L)} \tag{14}$$

where *ESQ* is the side length of the equivalent square field, W is the width of the rectangle, and L is the length of the rectangle.

This method of empirical compensation consists primarily of establishing a response correction factors table by the experimental approach. It is based on the separation of primary and scattering contribution parts of photons and electrons in the beam. However, the primary contribution part to the SSD cannot be evaluated through the measurement in the air as the local spectral variation in the air with respect to that in the water causes a large SSD response difference. Therefore, an arbitrary square field should be selected as a reference field for a given energetic beam. In this reference field, the maximum tissue ratio of SSD is compared with that measured of water by ionization chamber. Although it is possible to apply this method of compensation in irregular fields, it is difficult to implement it in more complex fields such as IMRT or non-rectangular fields, because this method requires a lot of effort for measuring, adjustments, and approximations that could be uneasy in more complex fields.

3.3.2 Cavity theory approach

The cavity theory was originally developed to convert the absorbed dose in the ionization chamber to the absorbed dose in the medium of interest [58]. When the measurement is performed with a solid-state dosimeter, the material of the detector, in general, is different from that of the medium in which it is introduced. If we consider the detector as a cavity introduced into the uniform medium of interest, the absorbed dose in the detector D_{det} is different with respect to the absorbed dose in the medium at this position in the absence of the detector, D_{med}. The main

objective of the cavity theory is to determine the response factor RF_Q, given by Eq. (15):

$$RF_Q = \left(\frac{D_{det}}{D_{med}}\right)_Q \tag{15}$$

where Q corresponds to a given beam quality. **Figure 6** illustrates the schematic application of cavity theory to convert detector absorbed dose for a given beam quality to the dose in the medium of interest by RF_Q [59].

There are two possible cavities where RF_Q could be derived, the large cavity and small cavity. The terms "small and large" refer to the size of the cavity relative to the bearing surfaces of secondary particles, i.e., the electrons and positrons.

3.3.3 Small cavity theory (SCT)

Small cavity theory is also referred to as Bragg-Gray cavity theory. First, William Bragg proposed it then Louis Harold Gray completed it [60]. Bragg-Gray proposed two conditions: (a) Cavity size should be small enough compared to the range of the charged particles inside the irradiated volume. So that, the fluence of charged particles and local fluence are not disturbed by the presence of the cavity in the middle (see **Figure 7**). (b) The absorbed dose in the cavity is completely deposited by charged particles which pass through the cavity.

The realization of the first condition ensures that the local influence is invariant, with or without the existence of this detector is to say $\Phi_{det}(E) = \Phi_{med}(E)$. The
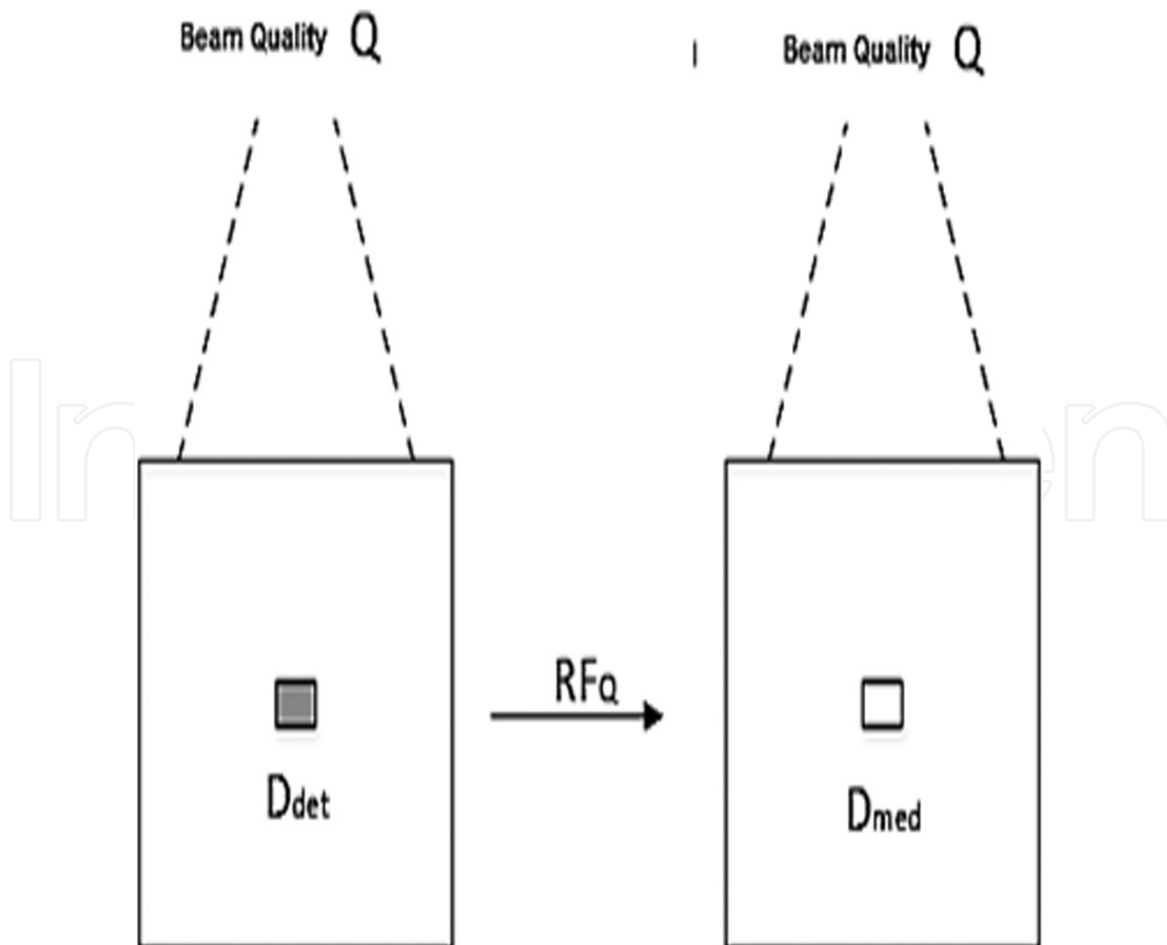
Figure 6.
Application of the cavity theory: The detector's absorbed dose for a given beam quality converted to the dose in the medium of interest by RF_Q [11].
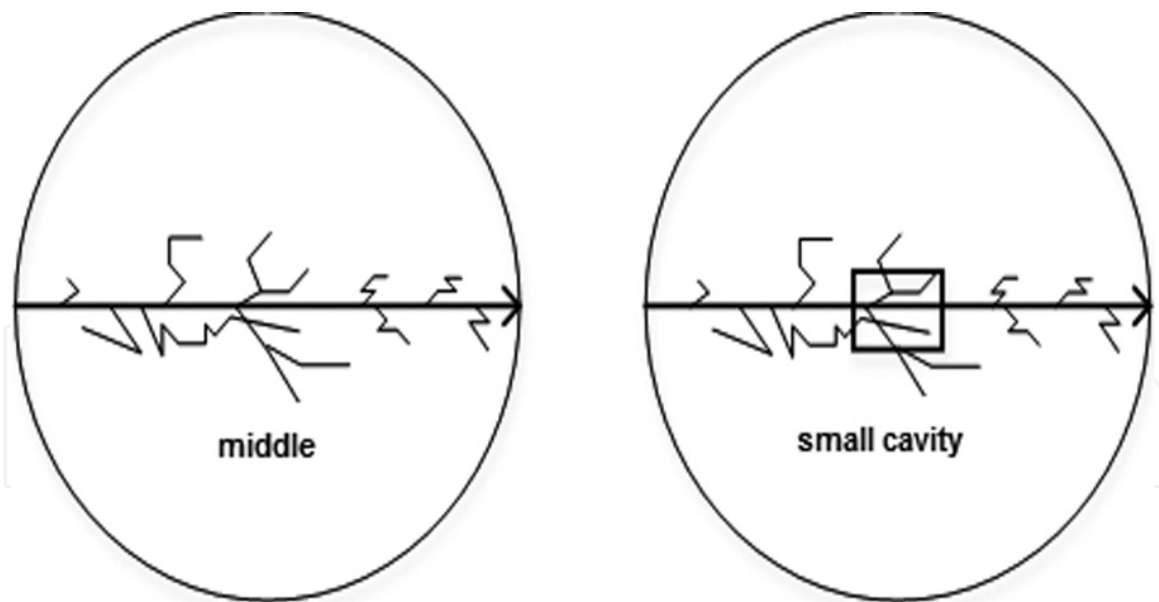
Figure 7.
A schematic illustration of small cavity behavior under high energetic photon irradiation.

second condition ensures that the dosimetric contribution from the photon is negligible. This is a valid condition for high-energy photon beams in most situations [61]. Under these conditions, D_{med} is related to D_{det} as:

$$\frac{D_{det}}{D_{med}} = \frac{\int_0^{E_{max}} \Phi_{med}(E)(S_{col}(E)/\rho)_{det} dE}{\int_0^{E_{max}} \Phi_{med}(E)(S_{col}(E)/\rho)_{med} dE} \qquad (16)$$

where $(s_{col}(E)/\rho)_{det}$ and $(s_{col}(E)/\rho)_{med}$ are collision stopping power of the detector and the medium, respectively, and E_{max} is the maximum energy in the spectrum of ionization chamber fluence.

Secondary particles (delta rays) are considered prerequisite to assess the dose by the stopping power that reaches a balance in the cavity. Another way to express this requirement is that the electron is considered to lose energy in the continuous slowdown cavity. However, it could generate high-energy secondary electrons by hard collisions in the cavity. These secondary electrons will come out of the cavity, and thus the delta ray balance is no longer valid. To take into account the effects of delta rays in an approximate way, Spencer and Attix proposed an extension of the cavity of theory [62]. Spencer-Attix theory considered the separation of electron particles into two parts: The fast electrons with an energy greater than a threshold (Δ) and slow electrons with energy below the threshold. Slow electrons are considered to deposit the energy locally inside the cavity, while the fast electrons are considered completely capable of crossing the cavity. The dose contribution by fast electrons is estimated by the restricted stopping power, $L_\Delta/\rho(E)$. The restricted stopping power is defined as the stopping power limited to lose energy below the threshold energy (Δ). The total dose in the cavity can be written as:

$$D = \int_\Delta^{E_{max}} \Phi(E)\left(\frac{L_\Delta(E)}{\rho}\right)dE + (E.T.) \qquad (17)$$

The first term on the right side of Eq. (17) corresponds to the dose deposited by fast electrons, and the second term takes into account the dose deposited by slow electrons, often termed as end track term (ET) suggested by Nahum [63] to estimate the contribution of slow electrons:

$$E.T. = \Phi(\Delta)\frac{S_{col}(\Delta)}{\rho}\Delta \tag{18}$$

where $\Phi(\Delta)$ is the electron differentiated fluence energy valued at Δ and $\frac{S_{col}(\Delta)}{\rho}$ is the nonrestricted stopping power evaluated at Δ. Instead of estimating the dose ratio in the detector and the medium by Bragg-Gray theory, it can be expressed as:

$$\frac{D_{det}}{D_{med}} = \frac{\int_0^{E_{max}} \Phi_{med}(E)(L_\Delta(E)/\rho)_{det}dE + \Phi(\Delta)(S_{col}(\Delta)/\rho)_{det}\Delta}{\int_0^{E_{max}} \Phi_{med}(E)(L_\Delta(E)/\rho)_{med}dE + \Phi(\Delta)(S_{col}(\Delta)/\rho)_{det}\Delta} \tag{19}$$

Δ is defined as the minimum energy needed for electron to pass through the cavity of interest. The value of Δ depends on the size and the material of the cavity. There are many studies based on determining Δ to apply the Spencer-Attix theory to some ionization chambers where Δ = 10 keV is used [64–66].

3.3.4 Large cavity theory (LCT)

On the other hand, large cavity is opposite to small cavity, whenever the size of the detector is much larger than the range of the electron that passes through the cavity. In this case, the range of delta ray is small in large cavity compared to the size of the cavity (see **Figure 8**). Hence, electronic equilibrium is established in most of the cavity size [59]. If the radiation source is a photon, it interacts with the material in the cavity and hence produces secondary electrons. As these created electrons are unable to pass through the cavity, the electronic control is established in the cavity of the detector. It should be noted that the electronic balance is not
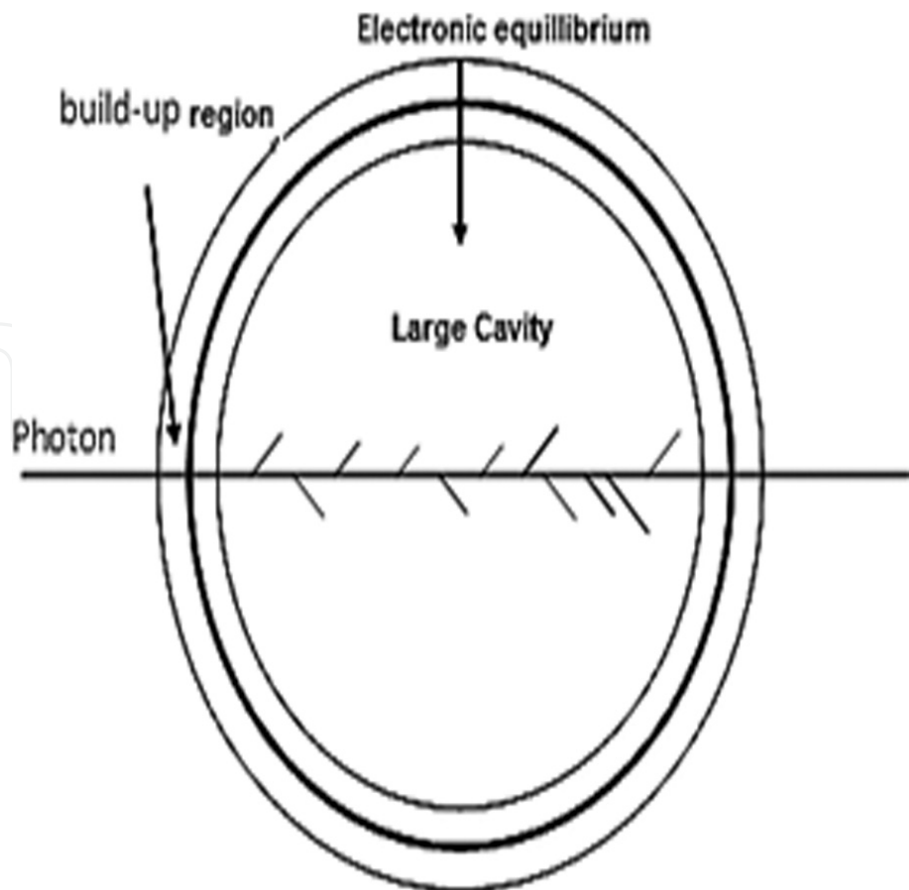
Figure 8.
Large cavity of high energetic photon beam deposition in a type of detector.

achieved in the border regions of the large cavity, due to the difference in the material around the border. However, the electronic balance is achieved in most of the cavity and the average absorbed dose in the detector can be determined using the following equation:

$$D = \int_0^{E_{max}} \left(\frac{\mu_{en}(E)}{\rho}\right)_{det} \cdot \Psi_{det}(E) dE \qquad (20)$$

where $(\mu_{en}(E)/\rho)_{det}$ is the mass absorption coefficient of the detector and $\Psi_{det}(E)$ is energy fluence of photon energy E in the detector.

3.4 Dose model for the SSD crystal in the photon beam

3.4.1 Spectrum convolution calculation

To apply cavity theory, the first step is to obtain the spectrum at the position of interest. Fluence pencil kernels may be used to calculate the local spectrum in a homogeneous phantom. This model had been extensively used to calculate the dose in treatment planning system (TPS) [55, 67–69]. Its idea is to convolute the energy depositions for each pencil beam energy through wide beam spectrum. The most interesting approach to pencil beam fluence has been proposed by [47, 70] which calculated the local spectra via dividing it into high and low energies using small and large cavity theory approximations, respectively. However, it could be easy to calculate other physical quantities, such as the fluence spectrum in an irradiated water phantom as in **Figure 9**. Eklund and Ahnesjö [28, 70] use fluence pencil kernel database to evaluate the spectrum. In this database, the fluence pencil kernel has been defined as the spatial distribution of fluence, resulted from the irradiation of semi-infinite water slab with point of the monodirectional and monoenergetic beam in water phantom of infinite thickness. Monte Carlo simulation had a good feature of interaction for the evaluation of these spectra. As the energy deposited in the phantom is laterally symmetric, the parameters to describe the fluence pencil can be reduced to three parameters, as shown in schematic geometry for fluence pencil kernel acquisition of monoenergetic beam (see **Figure 10**).
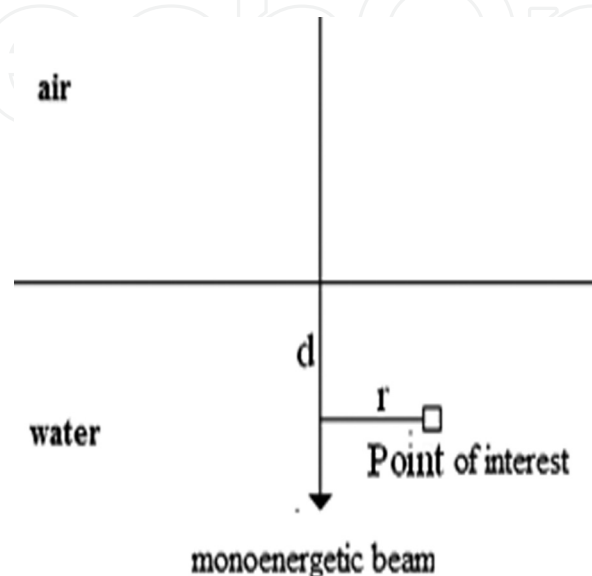
Figure 9.
A schematic geometry for fluence pencil kernel acquisition.
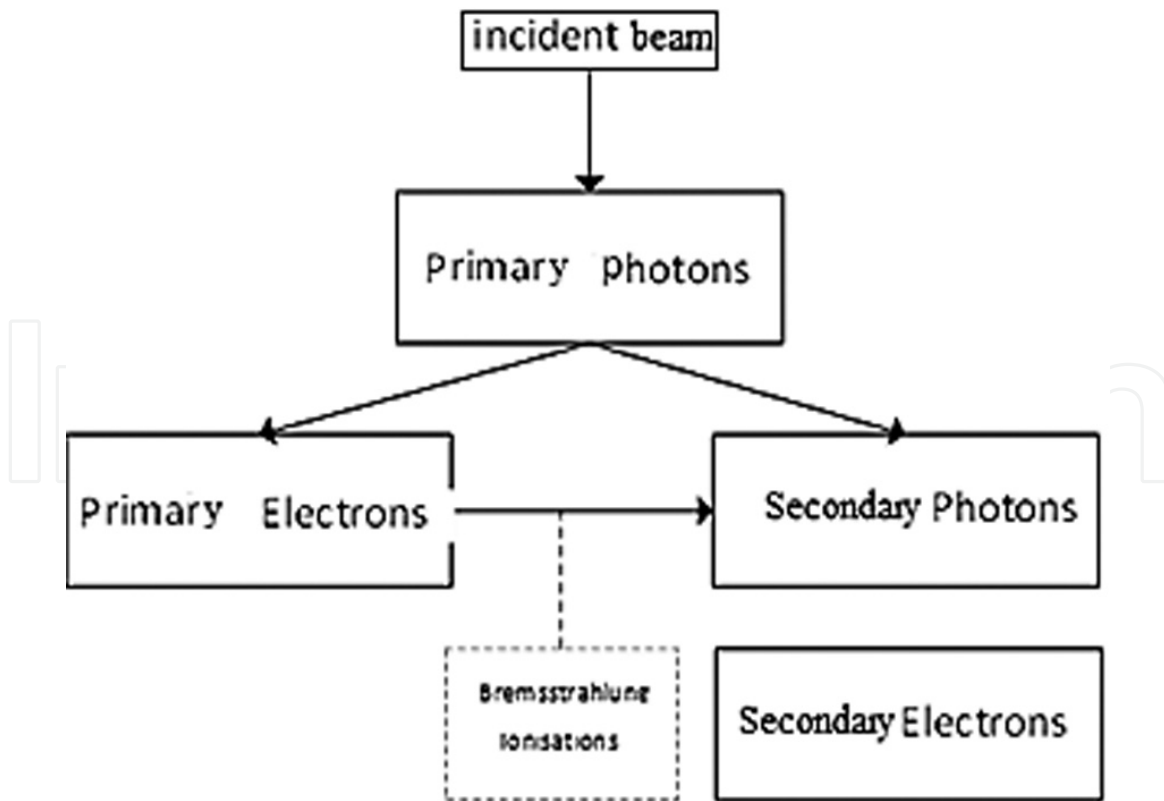
Figure 10.
Particles categories as defined in [70].

Here r is the lateral distance of the axis of irradiation from the position of interest; z is the depth of the point of interest; E is the energy of monoenergetic ionization chamber beam. Also, these database separated particles into four catego-ries, depending on their histories of interaction, as shown in **Figure 5**:

- The incident photons, without any interaction are primary photons.

- The electrons created in interactions of primary photons are primary electrons.

- All other photons are scattered that are created by primary photon or secondary electrons such as Rayleigh and Compton effect, bremsstrahlung, and pair production.

- The electrons created by the scattered photons are scattered electrons.

The first two types of particles (primary photons and electrons) are the main component of the beam, while the last two are the scattered component. This separation of particles is only possible with the feature of tracking the particle's interaction history in Monte Carlo simulation. To obtain the spectrum of charged particle fluence $\Phi_E(x, y, z)$ at the point of interest (x, y, and z) at a given irradiation field size, a convolution integration on energy is applied, as follows:

$$\Phi_E(x,y,z) = \int_0^{E_{max}} \iint \Psi(x',y',E)\phi(x-x',y-y',z,E)dx'dy'dE \qquad (21)$$

where $\Psi(x', y', E)$ is the lateral distribution photon energy fluence of the beam and $\phi(x - x', y - y', z, E)$ is the fluence pencil kernels to position (x, y, z). Note also

that $\Psi(x', y', E)$ may vary depending on the dose deposition in the irradiation field, which is the case of IMRT.

3.5 Response model of SSD

In reality, the response behavior of any dosimeter deviates in two cavity theories, because the extreme conditions for both theories are never completely filled. To determine if the dosimeter cavity is large or small, the size of the cavity is compared with the range of the electrons. If the dosimeter is irradiated with a polyenergetic beam, the cavity of theories cannot be applied directly due to the varied response to particles of different energies. In 2004, Yin et al. [30] proposed a method to treat the primary and scattered components separately by different cavity theories, assuming that the primary particles satisfy conditions of SCT while the scattered particles satisfy the LCT. The total dose measured in the Si-diode dosimeter [30] considered the sum of primary and scattered contributions using Eq. (22):

$$D^{cav} = \int_{\Delta}^{E_{max}} \Phi_{cav}^p(E) \cdot \frac{L_{\Delta}^{cav}(E)}{\rho} dE + \Phi_{cav}^p(\Delta) \cdot \frac{L_{\Delta}^{cav}(\Delta)}{\rho} \cdot \Delta + \int_0^{E_{max}} \Psi_{cav}^s(E) \cdot \frac{\mu_{en}^{cav}(E)}{\rho} dE$$

$$(22)$$

where $\Phi_{cav}^p(E)$ is the primary electron fluence and $\Psi_{cav}^s(E)$ is the energy of the scattered photon fluence. $\frac{L_{\Delta}^{cav}(E)}{\rho}$ is the restricted stopping power, and $\frac{\mu_{en}^{cav}(E)}{\rho}$ is the mass absorption coefficient of material in the cavity. This model proved quite precisely the dose in water, verified by measurement [27]. Eklund and Ahnesjö [26] introduced some solution to calculate dose response through the two assumptions: (1) Ensuring all primary electrons satisfy the SCT condition if the detector size is rather small. Nevertheless, there are still low-energetic electrons in the spectrum that cannot pass through the cavity of the dosimeter. (2) The scattered photons are considered to satisfy the condition of LCT, indicating that CPE is assumed to be located in the cavity of the dosimeter. The validity of this assumption depends on the energy of the scattered photon. To solve this situation, Eklund and Ahnesjö [71] introduced two solutions for the condition of the hypothesis is closer to reality: Instead of calculating the primary low-energetic electron contribution by LCT, they calculate the contribution from primary photons in LCT that create low-energetic primary electrons. From this calculation of the fluence spectra, it is possible to find the low-energetic primary photons. Therefore, a partitioning of the primary electrons was performed, where the high-energetic primary electrons followed the SCT and the contribution of low-energy electron primary was calculated using their father or primary photons. Ideally, the scattered photons should be partitioned in the same way to treat low component of high energy differently. $K(E)$ correction had been introduced, which is defined as follows:

$$K(E) = \frac{D_p^{cav}(E)}{\Psi(E) \cdot \frac{\mu_{en}^{cav}(E)}{\rho}}$$

$$(23)$$

where $D_p^{cav}(E)$ is the dose deposited in the cavity of the detector, by the primary photons of energy E (or primary electrons) with a fluence of photons $\Psi(E)$ and its primary electrons. The denominator of this expression represents the collision kerma of the cavity, which is equivalent to the dose if CPE exists locally. Computing $D_p^{cav}(E)$ is only possible by a total particle transport calculation as by Monte Carlo

simulation. With the introduction of partitioning primary electron and the approximation, factor CPE $K(E)$ in Eq. (21) gives:

$$D^{cav} = \int_{\Delta}^{E_{max}} \Phi_{cav}^{[E_A,E_{max}]p}(E) \cdot \left(\frac{L_{\Delta}^{cav}(E)}{\rho}\right) dE + \Phi_{cav}^{[E_A,E_{max}],p}(\Delta) \cdot \left(\frac{L_{\Delta}^{cav}(\Delta)}{\rho}\right) \cdot \Delta$$
$$+ \int_{0}^{E_{max}} K(E)\left(\Psi_{cav}^{[0,E_A],p}(E) + \Psi_{cav}^{s}(E)\right) \cdot \left(\frac{\mu_{en}^{cav}(E)}{\rho}\right) dE \qquad (24)$$

where $\Phi_{cav}^{[E_A,E_{max}]p}(E)$ is the fluence of primary electrons produced by the photon with a higher energy E_A and $\Psi_{cav}^{[0,E_A],p}(E)$ is the fluence of primary photons with smaller energy E_A. Applying Eq. (24), one can calculate the water dose, SSD dose, and response factor of Eq. (19). In order to compare the calculated response factor with the measured one, it is necessary to normalize the response factor determined for a reference, which gives:

$$RF_{norm}^{calc}(A,r) = \frac{RF^{calc}(A,r)}{RF^{calc}(A_{ref},r_{ref})} \qquad (25)$$

The reference value of field size is square field of 10 cm × 10 cm, and the reference position from the axis is at a depth of 10 cm in the phantom.

Crop et al. [2] had conducted one of the most detailed studies on the response of air-filled detectors in small photon beams. Author's considered the effect of different perturbation effects: (a) perturbation caused by differences in the composition of detector with respect to water (p_{wall}), (b) perturbation caused by replacement of water by detector ($p_{a,w}$), (c) effect caused by the existence of central electrode of the air-filled detectors, and (d) volume averaging effect for two detectors with different volume. The results of the study are illustrated in **Figure 11**; it was a Monte Carlo-based study for 6 MV photon beam considering photon beams down to 0.8 cm × 0.8 cm. The maximum variation was reported for P_{vol} and $P_{a,w}$.
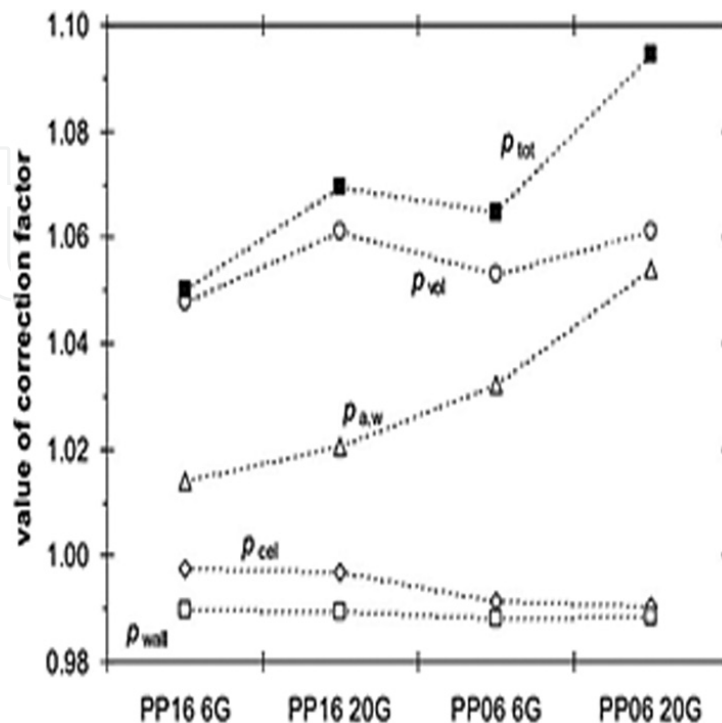
Figure 11.
Results reported by Crop et al. for different perturbation effects. Maximum deviation was reported for the volume averaging effect and perturbation caused by replacement of water by detector media.
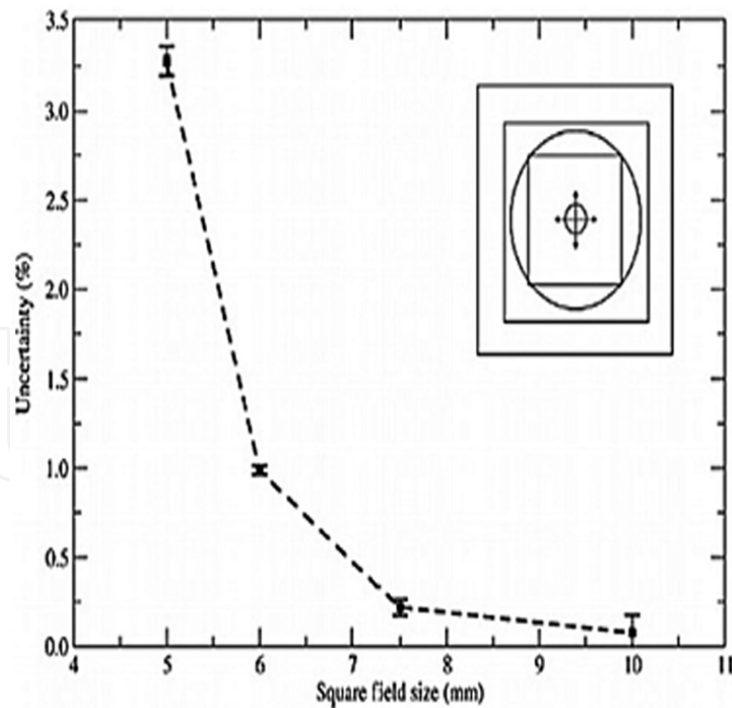
Figure 12.
Uncertainty observed in absorbed dose determination using PTW 60012 diode, due to uniformly distributed displacement error of 1 mm in all directions perpendicular to the beam axis.

In general case of large radiation beam, the value of total perturbation factor is approximately 0.99. However, for small photon beams, these perturbation factors become extremely large and no longer remain independent. Hence, Monte Carlo calculation of perturbation factors must be preferred over the use of SCT. Along with this, the size of the detector with respect to the source size and incorrect alignment can result in large values of correction factors. The perturbation caused by the displacement error in calculation of absorbed dose using Monte Carlo for PTW 60012 diode is illustrated in **Figure 12**. Similar results have been reported by various authors, for the Monte Carlo-based studies for computation of different perturbation factors [37, 72–77].

4. Energy spectrum and beam quality for small photon beams

4.1 Energy spectrum

The collimating devices utilized to project small photon beams result in blockage of photon source and scattered component of photon beam generated from the interaction of primary photon beam with other components of linear accelerator head, as a consequence of which the low energy photons are removed from the central axis of the beam. However, there may be probable increase in the amount of secondary component of beam for off-axis fields. The material composition of flattening filter is a deciding factor about whether the radiation beam will be softened or hardened. Along with this, there is a decrement in phantom scatter in small beams in comparison to the large field sizes. However, the decrement in phantom scatter is more noticeable than head scatter. Both effects are responsible for making the photon spectrum hard along the central axis of the beam. As a result the mass energy coefficient ratio and stopping power ratio of water and material of the detector are changed. Also in the small beams and the absence of LCPE, the

low-energy electrons reaching the axis of the beam will be reduced. Hence, the mean electron energy is increased, as a result of which stopping power ratio is also affected.

However, various Monte Carlo-based studies have revealed that the charged particle spectrum generated inside water is not much affected by the change in photon fluence. Hence, the stopping power ratio of water to air does not vary more than 0.5% at 10 cm of depth for 6 MV photon beam for field sizes ranging from 10 cm × 10 cm to 0.3 cm × 0.3 cm or circular fields of 0.3 cm diameter [78, 79], for depth ranging up to 30 cm maximum variation of 1% has been reported [70]. However, the response of diode detectors is affected by this hardening of the photon beam due to the noticeable change in the mass-energy absorption coefficient ratio of water and silicon. For field sizes ranging from 10 cm × 10 cm to 0.5 cm × 0.5 cm, the variation of 3–4% has been reported in the response of the unshielded diodes as a result of reduction in phantom scatter [71, 80].

4.2 Beam quality

For reference dosimetry in photon beams of high energy and large field sizes of beam quality Q using the air-filled detectors calibrated with respect to beam quality Q_0, the radiation quality correction factor k_{Q,Q_0} is required. There are two methods defined to account for beam quality [1, 3, 7]. First is the tissue phantom ratio at the depth of 20 and 10 g/cm^2 using water as a medium for 10 cm × 10 cm beam size and source-to-detector distance (SDD) of 100 cm, $TPR_{20,10}(10,10)_x$ [1]. The second method is based on percentage depth dose at a depth of 10 cm to 10 cm × 10 cm beam size and source to surface distance of 100 cm, $\%dd(10,10)_x$. These beam quality indices are utilized to calculate .

For some calibration laboratories, it is possible to provide calibration of air-filled detectors using clinical linear accelerator photon beam from calibration laboratories. This methodology for calibration of measurement equipment is much more realistic as there are small variations on the absorbed dose to water calibration factor for radiation equipment of the same kind, as the quality of beam varies moderately between the modern equipment of the same type. Therefore, it is possible to use the same radiation beam quality correction factor for similar model of air-filled detectors and radiation emitting equipment of the same kind. Hence, the dosimetric measurements on such machines can be performed without correction for beam quality. This methodology has been applied at some level for Gamma Knife® (Elekta AB, Stockholm), Cyberknife®, and TomoTherapy® (Accuray Inc., Sunnyvale, CA) radiation generators. Also, the components of the clinical linear accelerators such as secondary jaws and multi-leaf collimators are employed for having better machine uniformity and accurate small-field size definition [25–27]. It is important to remember that by the above method of calibration of equipment, there is no requirement for beam quality correction factors, and even then beam quality indices are crucial from commissioning and quality check procedure perspectives. Since the nominal photon beam energies used for intensity-modulated radiation therapy (IMRT), volumetric modulated arc therapy (VMAT), and stereotactic methods are below 10 MV, and the variation of $k_{Q,Q0}$ to quality of the beam is small [1, 2]. A large number of add-ons are utilized in IMRT and stereotactic radiotherapy treatment methods, which makes it impossible to prepare tables for beam quality correction factors for each and every combination of radiation emitters, add-ons, and detector types. Hence, $k_{Q,Q0}$ is not available in all machine/detector combinations. As a result the beam quality index or beam quality correction factor is required to relate the beam quality used for the detector calibration and the beam quality of the user machine. Since, it is sometimes not possible to

calibrate the detector in beam quality similar to that of user, and hence the values for all combination of machine/detector are not available. In that case the question arises, whether it is fine to use $TPR_{20,10}(10,10)_x$ or $\%dd(10,10)_x$ for dose measurements in fields smaller than 10 cm × 10 cm on the same radiation emitter. As discussed above the stopping power ratio variation with change in field size is small. Hence, the beam quality indices measured for large photon beams can be utilized for small beams. The variation of stopping power ratios with beam size and other perturbation factors can be merged together into an output correction factor.

In the conditions where the conventional beam size of 10 cm × 10 cm, a number of methods have been proposed to determine the beam quality:

a. A concept of machine-specific reference field (msr), f_{msr}, has been proposed by Alfonso et al. [81].

b. Machine-specific beam quality index has been proposed for TomoTherapy [82]. According to this methodology beam quality index is measured using similar methods as used for determination of the $\%dd(10, 10)_x$ in the conditions achievable in case of TomoTherapy. In this proposed methodology, authors calculated correction factors for beam quality with the help of Monte Carlo techniques and compared them with measurements as a function of conventional index to establish a relation between the machine-specific beam quality index and the conventional beam quality index [83].

c. In the third method, it is proposed to measure $TPR_{20,10}(S)$, the ratio of dose deposited at 20 and 10 g/cm² depths for an S cm × S cm square field size at source-to-detector distance of 100 cm. The measurement of $TPR_{20,10}(S)$ is performed on the machine where 10 cm × 10 cm field size is not achievable for series of square field sizes S, and comparison is made with the measurements performed using radiation emitter where 10 cm × 10 cm beam size is achievable; the measurement data is extrapolated [78, 79, 84]. Using this extrapolated data relationship for the beam quality index of 10 cm × 10 cm beam size, $TPR_{20,10}(10)$ and $TPR_{20,10}(S)$ are derived [85].

It was observed by Sauer et al. that the third methodology to measure beam quality index in nonstandard field sizes is effective for circular or rectangular fields using the concept of equivalent square field method [79, 85] and for flattening filter-free beams by surety of correction factor for deficiency in the lateral scatter because of conical beam profiles. It must be noted that the relation between the stopping power ratio and beam quality index in case of FFF radiation fields and WFF beams is not similar [86–89]. The relations to calculate $TPR_{20,10}(10)$ and $\%dd$ $(10,10)_x$ can be derived for small beams (S lying between 4 and 12 cm) [90]. **Figure 13** illustrated the variation of $TPR_{20,10}(S)$ for beam size of S cm × S cm for field sizes ranging from 4 cm × 4 cm to 12 cm × 12 cm with energy of photon beam ranging from 4 and 10 MV [79, 90] (squares representing the measurement data [79] and curved representing Monte Carlo results [90]).

4.3 Measurement of $TPR_{20,10}(10)$

The determination of $TPR_{20,10}(10)$ from the measurements obtained for $TPR_{20,10}(S)$, where S is the equivalent square f_{msr}, by using the measurement data in the analytic expression given by Palmans (Eq. (26)) [90]. **Figure 14** shows the experimental set-up to be used for measurement of $TPR_{20,10}(S)$, with source-to-detector distance of 100 cm and at a depth of 20 g/cm² and 10 g/cm².
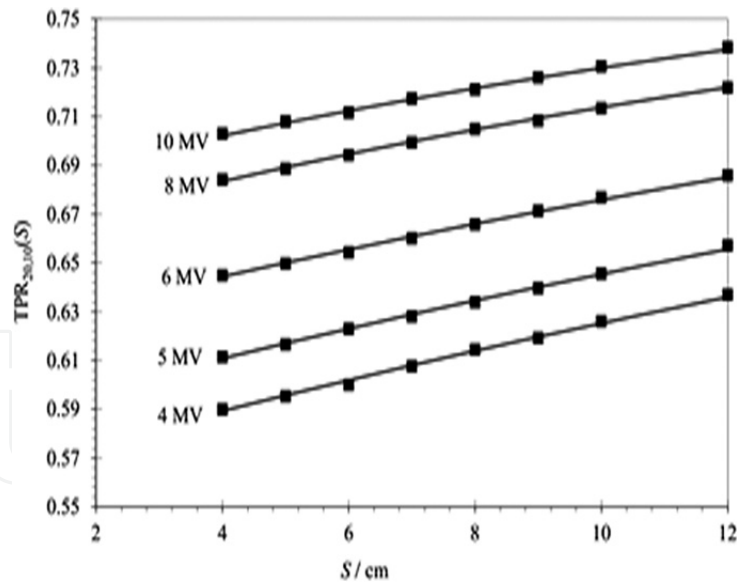
Figure 13.
Dependence of $TPR_{20,10}(S)$ on the field size S, for beam size ranging between 4 and 12 cm and photon energies between 4 and 10 MV.
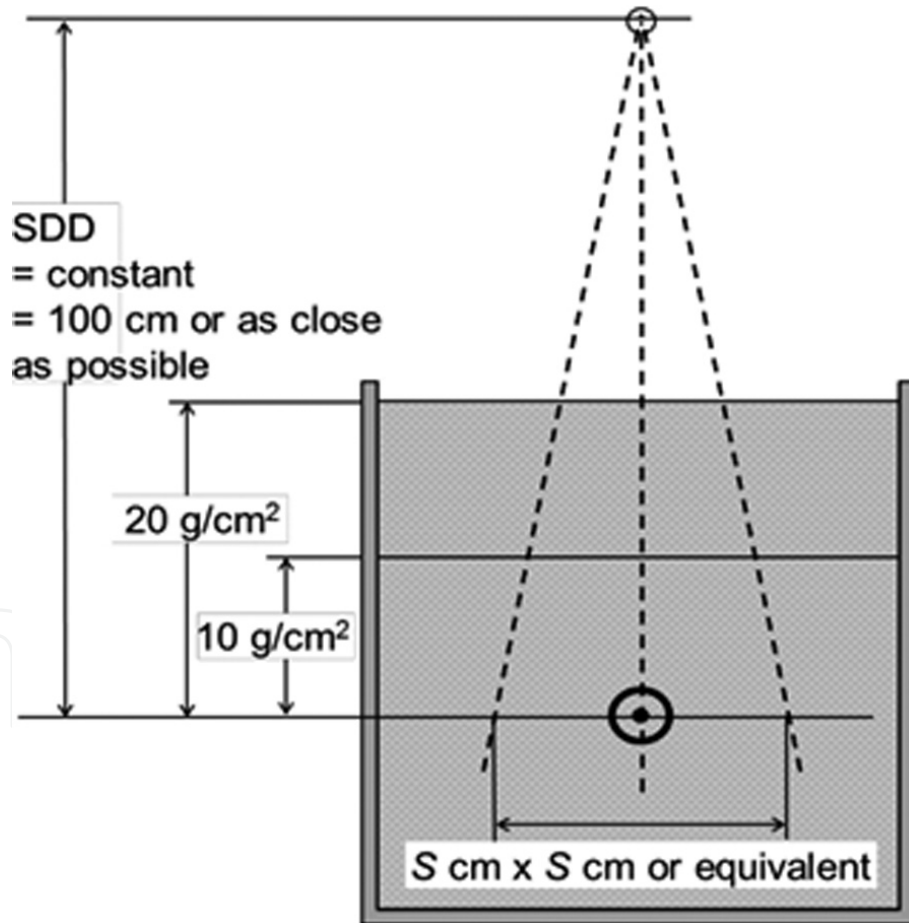
Figure 14.
The experimental set-up to be used for measurement of $TPR_{20,10}(S)$.

$TPR_{20,10}(10)$ for 10 cm × 10 cm can be derived using the following relationship:

$$TPR_{20,10}(10) = \frac{TPR_{20,10}(S) + c(10-S)}{1 + c(10-S)} \qquad (26)$$

This relation is valid when 4 cm $\leq$ S $\leq$ 12 cm, where C = $(16.15 \mp 0.12) \times 10^{-3}$.
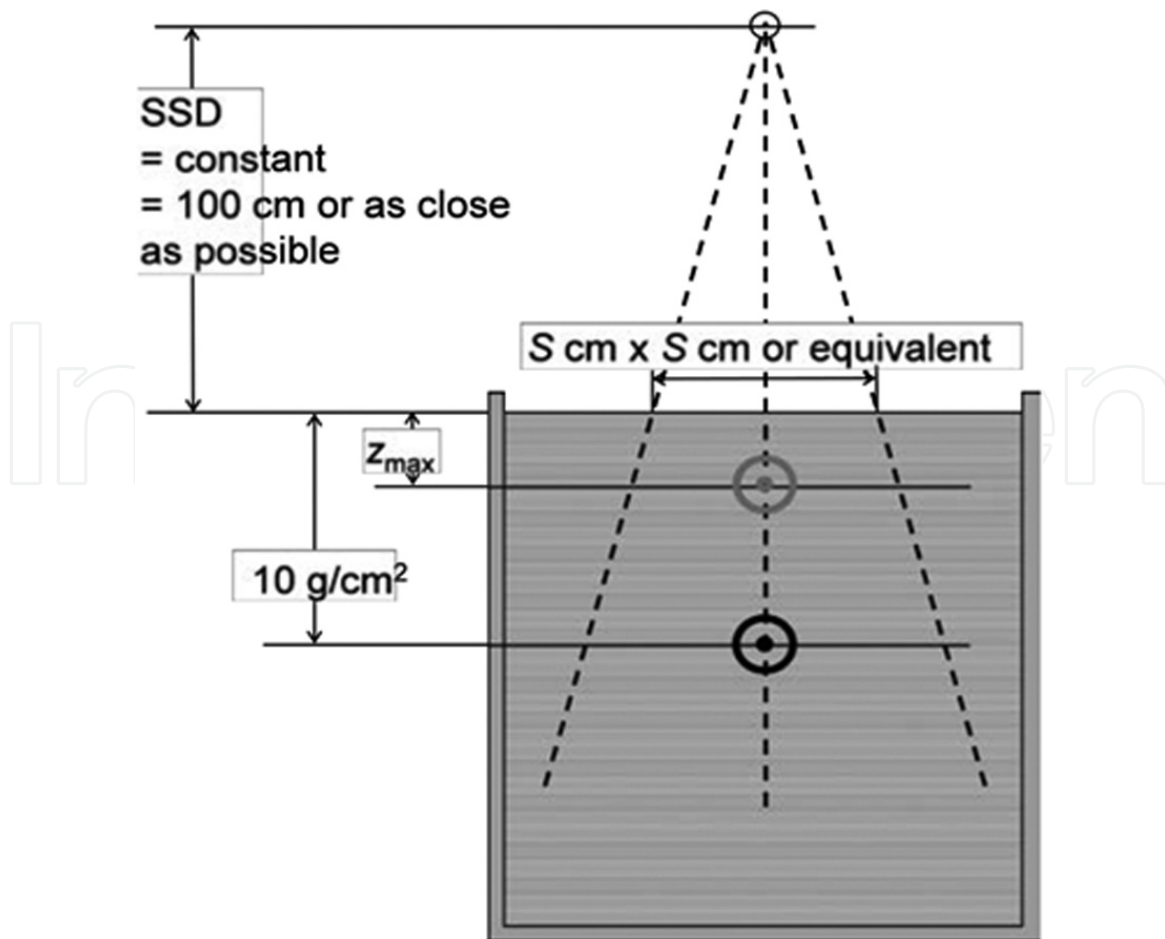
Figure 15.
Measurement setup for %dd(10,S).

4.4 Measurement of %dd(10,10)$_x$

Similar to the determination of $TPR_{20,10}(10)$ from measurements of $TPR_{20,10}(S)$, the %dd(10,10)$_x$ can be determined from the %dd(10) for S cm × S cm msr field size using the analytic relation provided by Palmans [90]. **Figure 15** illustrates the experimental setup for the measurement of %dd(10, S) for S cm × S cm beam size and measurement depths of maximum dose (z_{max}) and 10 g/cm^2 at a source-to-surface distance of 100 cm.

Lead foil is not required in the measurements of %dd(10,S) for WFF radiation beams (below 10 MV). However, the use of lead foil of 1 mm thickness is recommended for %dd(10,S) measurements in FFF radiation beams; in order to remove the electron contamination and analytic expression, Eq. (27) is used to calculate %dd(10,10)$_{Pb}$. Then %dd(10,10)$_x$ can be obtained from %dd(10,10)$_{Pb}$ using the relation provided by AAPM Task Group report 21.

The %dd(10,10)$_x$ can be calculated using the following expression:

$$\% \, dd(10, 10) = \frac{\% \, dd(10, S) + 80c(10 - S)}{1 + c(10 - S)} \tag{27}$$

where 4 cm $\leq$ S $\leq$ 12 cm and C = $(53.4 \mp 1.1) \times 10^{-3}$.

5. Determination of absorbed dose

In case of radiation-emitting equipment, where field beam of 10 cm × 10 cm (f_{ref}) can be established, the dose measurement is performed using the

recommendation provided by task group series (TRS) 398 and other equivalent protocols [1–7]. However, in radiation equipment where f_{ref} setting is not feasible, f_{msr} is used. The full width at half maximum of f_{msr} must satisfy small-field condition.

$$FWHM \geq 2\,r_{LCPE} + d \tag{28}$$

5.1 Measurement of absorbed dose in f_{msr}

5.1.1 Calibration coefficient for f_{msr} is available

In situations where calibration coefficient in terms of absorbed dose to water $(N_{D,w,Q_{msr}}^{f_{msr}})$ is available for machine-specific reference field (f_{msr}) and beam quality similar to that of the user beam (Q_{msr}), the absorbed dose to water at depth of reference (z_{ref}) in the nonexistence of detector in water can be determined using the following relation:

$$D_{w,Q_{msr}}^{f_{msr}} = M_{Q_{msr}}^{f_{msr}} N_{D,w,Q_{msr}}^{f_{msr}} \tag{29}$$

where $M_{Q_{msr}}^{f_{msr}}$ is the detector reading f_{msr} beam corrected for influential quantities, such as temperature, pressure, perturbation factors, etc.

5.1.2 Calibration factor available for f_{ref} (10 cm × 10 cm) and beam quality (Q_0) correction factor

In conditions where calibration coefficient $(N_{D,w}^{f_{ref}})$ is provided by calibration laboratory in terms of f_{ref} and correction factor quality of beam Q_0. The absorbed dose to water can be calculated using the following relation:

$$D_{w,Q_{msr}}^{f_{msr}} = M_{Q_{msr}}^{f_{msr}} N_{D,w,Q_0}^{f_{ref}} k_{Q_{msr},Q_0}^{f_{msr},f_{ref}} \tag{30}$$

where $M_{Q_{msr}}^{f_{msr}}$ is the detector reading reworked for influential quantities and $k_{Q_{msr},Q_0}^{f_{msr},f_{ref}}$ is the correction factor for difference in beam quality and field size.

5.1.3 Calibration factor available for f_{ref} (10 cm × 10 cm) without beam quality (Q_0) correction factor

In the situation where the correction factor for the generic quality of beam, correcting for the difference in beam quality and effect of difference in field size, is not provided by the calibration laboratory, the dose deposited can be determined using the following relation:

$$D_{w,Q_{msr}}^{f_{msr}} = M_{Q_{msr}}^{f_{msr}} N_{D,w,Q_0}^{f_{ref}} k_{Q,Q_0}^{f_{ref}} k_{Q_{msr},Q}^{f_{msr},f_{ref}} \tag{31}$$

where $M_{Q_{msr}}{}^{f\,msr}$ is the detector reading for f_{msr} reworked for influential quantities, $N_{D,w,Q_0}{}^{f\,ref}$ is the detector calibration factor in terms of absorbed dose to water in f_{ref} beam and Q_0 quality of beam, $k_{Q,Q_0}{}^{f\,ref}$ is the correction factor for difference in detector response of detector in beam quality Q_0 in field size f_{ref} and response of detector in beam quality Q in f_{ref} beam size, and $k_{Q_{msr},Q}{}^{f\,msr,\,f\,ref}$ is the beam quality correction factor to account for the difference between the response of detector in beam quality Q, f_{ref} beam size and beam quality Q_{msr}, and beam size of f_{msr}.

In order to determine the dose deposited in water for FFF radiation beam, the following relation can be used:

$$D^{f\,msr}{}_{w,Q_{msr}}{}^{FFF} = M^{f\,msr}{}_{Q_{msr}}{}^{FFF} N_{D,w,Q_0}{}^{f\,ref} k_{Q^{WFF},Q_0}{}^{f\,ref} k_{Q^{FFF},Q^{WFF}}{}^{f\,ref} k_{Q_{msr},Q}{}^{f\,msr,\,f\,ref} \quad (32)$$

where $k_{Q^{WFF},Q_0}{}^{f\,ref}$ is the correction for beam quality for difference in response of the detector in beam Q^{WFF}, beam size f_{ref} and response of detector in quality of beam Q_0, and beam size of f_{ref}. It can be taken from the international dosimetry protocols [1, 2, 7], and $k_{Q^{FFF},Q^{WFF}}{}^{f\,ref}$ is the factor of correction for variation in response of the detector in the FFF and WFF radiation fields. It can be obtained from Monte Carlo studies. **Figure 16** summarizes the different conditions discussed above for the determination of dose deposited in water.
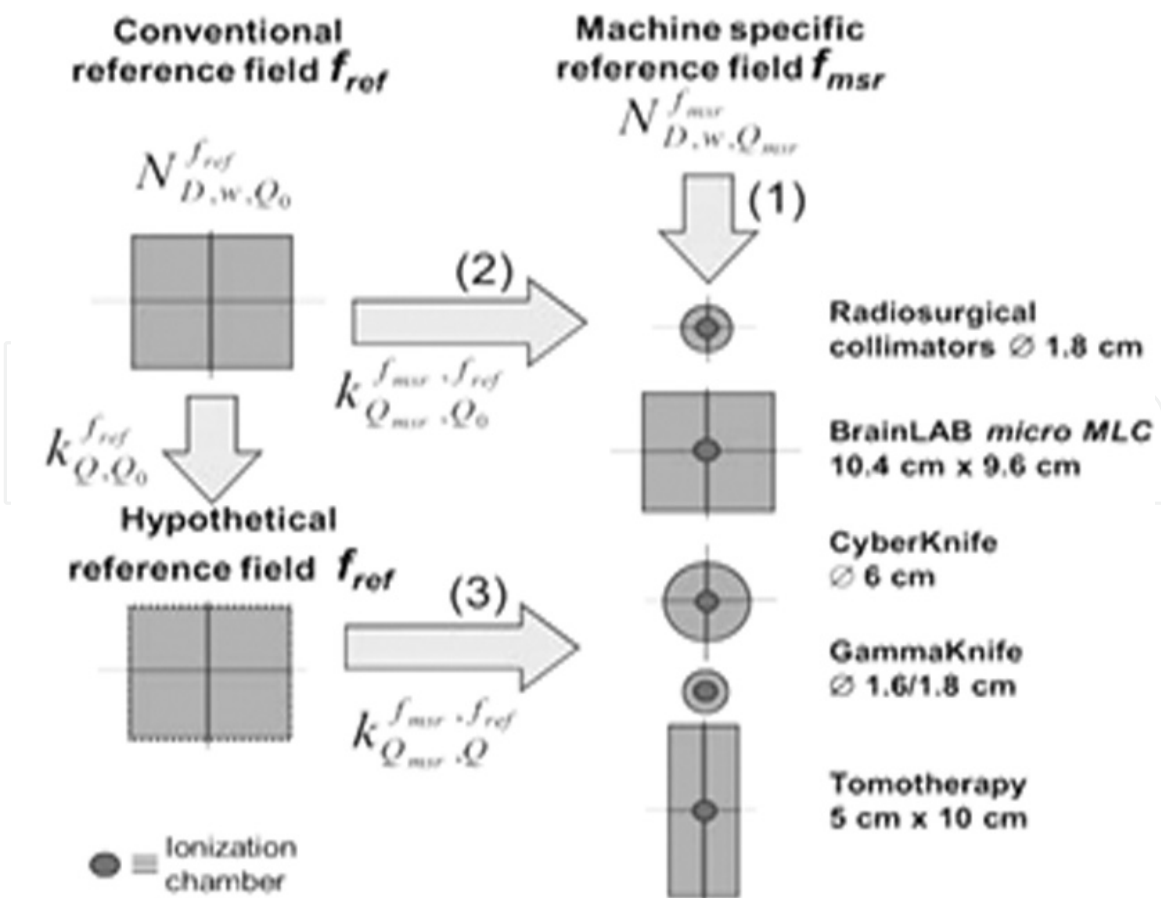
Figure 16.
Schematic summary of the determination of absorbed dose in case of small beams considering the case of machine specific reference field according to the formalism given by TRS 483. The arrows and formulas labeled (1), (2) and (3) refer to Section 6.1.1, 6.1.2 and 6.1.3, respectively.

5.2 Measurement of field output factors

To measure the dose deposited by clinical radiation beams with respect to the msr field in Ref. dosimetry, field output factors ($\Omega_{\Omega_{clin}\Omega_{msr}}^{f_{clin}f_{msr}}$) are determined. They are also known as relative dose factors [91] or total scatter factors [1, 56, 79]. It is defined as the ratio of dose deposited in water by clinical beam (f_{clin}) with the quality of beam (Q_{clin}) to the dose deposited in water in msr field (f_{msr}) with quality of beam Q_{msr}:

$$\Omega_{\Omega_{clin}\Omega_{msr}}^{f_{clin}f_{msr}} = \frac{D_{w,Q_{clin}}^{f_{clin}}}{D_{w,Q_{msr}}^{f_{msr}}} \tag{33}$$

The output factors are utilized to calculate the dose deposited to water in clinical beams (f_{clin}) from the dose deposited to water in machine-specific reference beams (f_{msr}). $\Omega_{\Omega_{clin}\Omega_{msr}}^{f_{clin}f_{msr}}$ can be determined using the detector readings by using the following relation:

$$\Omega_{\Omega_{clin}\Omega_{msr}}^{f_{clin}f_{msr}} = \frac{M_{Q_{clin}}^{f_{clin}}}{M_{Q_{msr}}^{f_{msr}}} k_{Q_{clin},Q_{msr}}^{f_{clin},f_{msr}} \tag{34}$$

where $k_{Q_{clin},Q_{msr}}^{f_{clin},f_{msr}}$ is the output correction factor; it can be determined either by direct measurements or using Monte Carlo techniques.

6. Monte Carlo simulation in small-field dosimetry

Monte Carlo techniques are widely used as an alternative in situations where measurements are either difficult or are not possible. Many authors have reported about the possibility of using MC techniques for small-field dosimetry [92–98]. Monte Carlo techniques can be used to calculate the correction factors as discussed in Section 6 of this chapter. It can also be used as a reference or standard with respect to different techniques of relative and absolute dose measurements with acceptable accuracy. With the use of Monte Carlo techniques, the dosimetry in low-density materials can be understood where it is difficult to perform measurements due to the presence of non-equilibrium conditions [99–105]. In radiation dosimetry two approaches are followed for the use of MC techniques. First approach is to calculate correction factors for the dosimeters to be used for dosimetric measurements. In the second approach, the dosimetric quantities are directly calculated, which is equivalent to performing measurements in ideal conditions. However, it is important to verify the MC model against the beam modeling parameters before using it for radiation dosimetry calculations.

6.1 General purpose of Monte Carlo codes for radiation dosimetry

It is possible to explicitly model the interaction of every particle using Monte Carlo techniques. The main characteristics of Monte Carlo techniques used for radiation dosimetry are:

1. The generation of particles is based on the distribution function used to describe the radiation source.

2. The random numbers are obtained in the range of (0, 1) using the pseudorandom number generators.

3. The probability distribution functions are sampled using interaction cross sections.

4. The step of a particle is defined as the distance between two consecutive events (collision/scatter).

5. "Scoring" for each and every outcome is performed to calculate quantities, such as dose deposited in a medium.

6. In order to reduce the statistical uncertainty in the calculation, it is recommended to perform simulations using a large number of particles ($\sim 1 \times 10^9$).

There are various Monte Carlo codes available which can be used in radiation dosimetry of stereotactic fields. The most commonly used MC codes are Electron Gamma Shower [106], GEANT4 [107], and the Monte Carlo N-Particle code [108]. Due to highly accurate radiation transport algorithm for electrons and photons and easy to use BEAM package, EGSnrc is one of the most frequently used Monte Carlo codes for small-field dosimetry.

6.2 Monte Carlo studies for small-field dosimetry

Heydarian et al. [109] performed a study using diamond detectors, diodes, films, and EGS4 Monte Carlo code, for field sizes ranging from 7 to 23 mm on Siemens Mevatron linac. Scielzo et al. [110] investigated the application of Monte Carlo-based calculation algorithm for treatment planning in stereotactic radiosurgery for Varian 2100C. Authors reported large difference between the treatment planning system (TPS) and MC calculation, especially near the inhomogeneous regions. Verhaegen et al. [92] performed a dosimetric study using the BEAM/EGS4 Monte Carlo code for 6 MV SRS unit for circular field sizes with diameter ranging from 1.25 to 5 cm at isocenter. The authors reported a good agreement between the measurement and computational results for most of the detectors in terms of cone factor. De Vlamynck et al. [111] performed clinical dosimetry using Markus parallel plate ion chamber and diamond detector in 6 MV photon beam of SL 25 (Elekta) linac and compared the results with Monte Carlo calculations. The depth dose distributions for measured and calculated data were found in good agreement with each other; however slight discrepancies were reported for lateral beam profiles. Cheung et al. [112] verified the accuracy of treatment planning system (Leksell GammaPlan) using Gafchromic films and Monte Carlo methods for field sizes ranging from 4 to 18 mm on a Gamma Knife unit. Variations up to 10% were observed for Gafchromic films which were attributed to the energy dependency of films. Westermark et al. [113] performed a comparative study using diamond detector, liquid ion chamber, plastic scintillator, silicon diode, and Monte Carlo techniques for small-field sizes ($\varphi > 4$ mm) of 6 and 18 MV photon beams in order to study the response of various dosimeters. Deng et al. [114] generated a multiple source model by following the procedure of beam commissioning for Cyberknife unit for Monte Carlo-based treatment planning. Authors reported largest variation of 9.5% for ionization

chamber IC-10 and attributed this variation to the volume averaging effect of the chamber. Paskalev et al. [115] investigated the dose distribution for circular field (1.5 and 3 mm) for 10 MV photon beam using Varian Clinac-18 and reported maximum variation of 0.3 mm between the measured and calculated 50% isodose surface. Tsougos et al. [116] performed a Monte Carlo-based dosimetric study for in-house developed 6 MV SRT unit and compared it against conventional dosimetric techniques. Francescon et al. [117] investigated total scatter factor for Cyberknife unit for three different collimator opening diameters ranging from 5 to 10 mm. Comparison was made between the experimental and Monte Carlo results. Heydarian et al. [118] investigated the dosimetric parameters of a SRS linac using experimental measurements and Monte Carlo methods and reported good agreement between the Monte Carlo and experimental data. Scott et al. [29] investigated the effect of source occlusion on output of the linac for small-field sizes and large focal spot sizes and found that output factors are sensitive to the dimensions of the electron spot size hitting the target. Sargison et al. [119] proposed a methodology for measurement and reporting of relative output factors for small fields using both experimental and Monte Carlo methods. In 2014, Sargison et al. [120] presented two scientific quantitative definitions of very small-field size and reported that careful methodology is required for setting of field sizes and placement of detectors for field sizes less than 12 mm for 6 MV photon beams. In 2019, Francescon et al. [121] investigated the sensitivity of dosimetric correction factors to interunit variation and reported variation up to 9% between the measured data corrected using the recommendations of TRS-483 and Monte Carlo results. Casar et al. [122] provided detector-specific output correction factors for small-field sizes using the recommendations of TRS-483.

6.3 Monte Carlo codes optimized for radiation therapy and out-of-field doses for small fields

Considering the ability of Monte Carlo techniques to calculate absorbed dose in non-equilibrium conditions, it can be an ideal tool for clinical use. However, due to its lengthy computational sessions, it is difficult to use them in clinic. In the above section, we discussed about the general purpose of Monte Carlo tools which can model different types of particles (gamma, electron, positron, etc.) and different kinds of physics models to simulate the interactions of particles over the large range of energy of incident particles. The introduction of Monte Carlo-based treatment planning systems, which uses some approximations and simplification in comparison to full Monte Carlo codes, can help to overcome the limitations of contemporary TPS. In Monte Carlo-based TPS, a part of dose calculation is performed using Monte Carlo methods, and the remaining part is performed using approximation-based algorithms [123, 124]. Another option is to use Monte Carlo codes that are optimized specially for radiation therapy applications. TG105 report can provide more information about the use of Monte Carlo methods for clinical applications [125]. However, it is possible that the highly efficient Monte Carlo codes that can completely simulate the radiation transport within acceptable timeframe will be still required. Hence, the use of Monte Carlo methods in small-field dosimetry will increase the confidence in the accuracy of calculation of dose distributions.

Apart from the difficulty in calculating dose deposited within the field, TPS algorithms are also not able to calculate the doses out-of-field accurately, since the measurement data obtained to be used for commissioning of TPS extends only a few centimeters beyond the edges of the field. Penumbra region is defined as a region of steep dose fall, where radiation dose falls from 80 to 20% of maximum dose within the field. The dose protruding beyond the field is not considered in the calculation

of the dose distribution or its contribution to the procedure of inverse optimization. Hence, the dose distribution obtained from TPS is expected to be inaccurate in regions beyond the edges of the primary field. The predictions in low-dose regions near the primary field by TPS have been shown to be inaccurate as well. Jang et al. [126] investigated the inaccuracies in dose calculation in low-dose regions for intensity-modulated radiotherapy (IMRT) and reason behind these inaccurate calculations by comparing their results against Monte Carlo methods. Authors reported error up to 25% in low-dose regions and found that the inadequate modeling of transmission through MLC leaves and leaf scatter in TPS to be the main cause of error. In the treatments performed using IMRT techniques, doses of 2 Gy per fraction is delivered over large fractions to deliver a total dose of 60–70 Gy to the tumor volume. However, stereotactic radiotherapy follows hypofractionated regime, in which doses of 10–20 Gy per fraction is delivered. Hence, the dose deposited out-of-field due to each fraction is of concern. Petti et al. [127] investigated the doses outside the treatment field and cause of it for treatment using Cyber Knife and compared them against the doses obtained using Gamma Knife and IMRT for similar treatment. The out-of-field doses were found higher by a factor of two to five for Gamma Knife and by a factor of four for IMRT treatments. According to the authors, the leakage radiation is the main cause of out-of-field doses. Chuang et al. [128] investigated for the reduction in out-of-field doses after installation of shielding upgrade and reported the reduction of 20–50% in out-of-field doses. Comparison of difference in peripheral doses absorbed using different equipment for stereotactic treatment was made by Di Betta et al. [129] and used the data for estimation of risk of stochastic effects. Authors reported that the risk of adverse side effects for treatment using 5 Gy per fraction due out-of-field doses is negligible. Lastly, there are relatively fewer studies available on out-of-field doses due to the small fields. More studies are required on it, which can be helpful to investigate the effects of out-of-field doses.

7. Conclusion

Considering the importance of accurate small-field dosimetry, this chapter discusses all important aspects related to it in details. It includes the physics of small radiation fields, cavity theory, and methodology of small-field dosimetry to understand the response of dosimeters and brief discussion on several dosimeters. It also discusses the recommendations of COP for dosimetry of small radiation fields. Moreover, it discusses the small and long cavity theories for computing the accurate dose response. In addition, pencil beam algorithms as a tool for the dose response evaluation is reported, and uses of Monte Carlo simulation in categorizing the primary and scattering components of the radiotherapeutic photon beam are handled. Also this chapter focuses on the application and importance of Monte Carlo techniques in small-field dosimetry and treatment methods that are based on small fields, such as stereotactic treatments and IMRT. Available general purpose Monte Carlo codes used for applications in radiotherapy is also mentioned. Such Monte Carlo codes have the ability to simulate transport of radiation within a medium in great details. EGSnrc, Geant4, PENELOPE, and MCNP are some of the most commonly used Monte Carlo codes for small-field dosimetry studies. Its accurate algorithm to model the transport of radiation and easy-to-use graphical user interface of BEAM code of EGSnrc makes it one of the most widely used MC code. A thorough recent literature review is performed on the small-field dosimetric studies performed using Monte Carlo codes. The studies on out-of-field doses, limitation of contemporary treatment planning systems, use of Monte Carlo codes

optimized specially for their use in radiation therapy simulation, and need of use of full Monte Carlo for dose calculations are also reviewed. It was concluded that still more studies on these issues are required in order to investigate the effects related to inaccurate dosimetry in depth. Hence, it can be concluded from the above discussion that the user must select a suitable dosimeter and follow the recommendations provided by TRS-483 for accurate beam data collection and accurate dosimetric measurements.

Author details

Hossam Donya[1,2*], Baljeet Seniwal[3], Reem Darwesh[1] and Telma C.F. Fonseca[3,4]

1 Department of Physics, Faculty of Science, King Abdulaziz University, Jeddah, Saudi Arabia

2 Physics Department, Faculty of Science, Menoufia University, Shebin El-Koom, Egypt

3 Programa de Pós-graduação em Ciências e Técnicas Nucleares - UFMG BH/MG, Brasil

4 Departamento de Engenharia Nuclear — DEN BH/MG, Brasil

*Address all correspondence to: hdunia@kau.edu.sa; donyavip@yahoo.com

References

[1] Godson HF, Ravikumar M, Ganesh KM, Sathiyan S, Ponmalar YR. Small field output factors: Comparison of measurements with various detectors and effects of detector orientation with primary jaw setting. Radiation Measurements. 2016;**85**:99-110

[2] Crop F, Reynaert N, Pittomvils G, Paelinck L, De Wagter C, Vakaet L, et al. The influence of small field sizes, penumbra, spot size and measurement depth on perturbation factors for microionization chambers. Physics in Medicine & Biology. 2009;**54**(9):2951

[3] Institute of Physics and Engineering in Medicine. Small Field MV Photon Dosimetry, IPEM Rep. 103. York: IPEM; 2010

[4] McEwen M et al. Addendum to the AAPM's TG-51 protocol for clinical reference dosimetry of high-energy photon beams. Medical Physics. 2014;**41**:041501

[5] Lillicrap SC, Owen B, Williams JR, Williams PC. Code of practice for high-energy photon therapy dosimetry based on the NPL absorbed dose calibration service. Physics in Medicine and Biology. 1990;**35**:1355-1360

[6] International Atomic Energy Agency. Absorbed Dose Determination in External Beam Radiotherapy: An International Code of Practice for Dosimetry Based on Standards of Absorbed Dose to Water, Technical Reports Series No. 398. Vienna: IAEA; 2000

[7] Netherlands Commission on Radiation Dosimetry. Code of Practice for the Absorbed Dose Determination in High Energy Photon and Electron Beams, Rep. NCS-18. Delft: NSC; 2008

[8] Andreo P. Monte Carlo simulations in radiotherapy dosimetry. Radiation Oncology. 2018;**13**(1):121

[9] IAEA. Dosimetry of Small Static Fields Used in External Beam Radiotherapy: An International Code of Practice for Reference and Relative Dose Determination. IAEA; 2017

[10] Das IJ, Ding GX, Ahnesjö A. Small fields: Nonequilibrium radiation dosimetry. Medical Physics. 2008;**35**: 206-215

[11] Papaconstadopoulos P. On the detector response and the reconstruction of the source intensity distribution in small photon fields [PhD thesis]. Montreal, Canada: McGill University; 2016

[12] Kalach NI, Rogers DW. Which accelerator photon beams are 'clinic-like' for reference dosimetry purposes? Medical Physics. 2003;**30**:1546-1555

[13] Wuerfel J. Dose measurements in small fields. Medical Physics International. 2013;**1**:81-90

[14] Ralston A, Liu P, Warrener K, McKenzie D, Suchowerska N. Small field diode correction factors derived using an air core fibre optic scintillation dosimeter and EBT2 film. Physics in Medicine and Biology. 2012;**57**: 2587-2602

[15] Sibata CH, Mota HC, Bedder AS, Higgins PD, Shin KH. Influence of detector size in photon beam profile measurements. Physics in Medicine and Biology. 1991;**36**:621-631

[16] Higgins PD, Sibata CH, Siskind L, Sohn JW. Deconvolution of detector size effect for small field measurement. Medical Physics. 1995;**22**:1663-1666

[17] Garcia-Vicente F, Delgado JM, Peraza C. Experimental determination of the convolution kernel for the study of the spatial response of a detector. Medical Physics. 1998;**25**:202-207

[18] Pantelis E et al. Dosimetric characterization of CyberKnife radiosurgical photon beams using polymer gels. Medical Physics. 2008;**35**: 2312-2320

[19] Azangwe G et al. Detector to detector corrections: A comprehensive experimental study of detector specific correction factors for beam output measurements for small radiotherapy beams. Medical Physics. 2014;**41**:072103

[20] McEwen MR. Measurement of ionization chamber absorbed dose kQ factors in megavoltage photon beams. Medical Physics. 2010;**37**: 2179-2193

[21] Georg D, Knöös T, McClean B. Current status and future perspective of flattening filter free photon beams. Medical Physics. 2011;**38**:1280-1293

[22] Pantelis E et al. On the implementation of a recently proposed dosimetric formalism to a robotic radiosurgery system. Medical Physics. 2010;**37**:2369-2379

[23] Kawachi T et al. Reference dosimetry condition and beam quality correction factor for CyberKnife beam. Medical Physics. 2008;**35**:4591-4598

[24] Le Roy M et al. Assessment of small volume ionization chambers as reference dosimeters in high-energy photon beams. Physics in Medicine and Biology. 2011;**56**:5637-5650

[25] Li XA, Soubra M, Szanto J, Gerig LH. Lateral electron equilibrium and electron contamination in measurements of head-scatter factors using miniphantoms and brass caps. Medical Physics. 1995;**22**:1167-1170

[26] Laub WU, Wong T. The volume effect of detectors in the dosimetry of small fields used in IMRT. Medical Physics. 2003;**30**:341-347

[27] Eklund K, Ahnesjö A. Modeling silicon diode energy response factors for use in therapeutic photon beams. Physics in Medicine and Biology. 2009; **54**:6135-6150

[28] Eklund K. Modeling silicon diode dose response in radiotherapy fields using fluence pencil kernels [PhD thesis]. Uppsala, Sweden: Uppsala University; 2010

[29] Scott AJ, Nahum AE, Fenwick JD. Monte Carlo modeling of small photon fields: Quantifying the impact of focal spot size on source occlusion and output factors, and exploring miniphantom design for small-field measurements. Medical Physics. 2009; **36**:3132-3144

[30] Yin Z, Hugtenburg R, Beddoe AH. Response corrections for solid-state detectors in megavoltage photon dosimetry. Physics in Medicine and Biology. 2004;**49**:3691-3702

[31] McKerracher C, Thwaites DI. Verification of the dose to the isocentre in stereotactic plans. Radiotherapy and Oncology. 2002;**64**:97-107

[32] Betzel GT, Lansley SP, Baluti F, Reinisch L, Meyer J. Clinical investigations of a CVD diamond detector for radiotherapy dosimetry. Physica Medica. 2012;**28**:144-152

[33] Ciancaglioni I et al. Dosimetric characterization of a synthetic single crystal diamond detector in clinical radiation therapy small photon beams. Medical Physics. 2012;**39**:4493-4501

[34] Marsolat F et al. A new single crystal diamond dosimeter for small beam: Comparison with different commercial active detectors. Physics in Medicine and Biology. 2013;**58**:7647-7660

[35] Ralston A, Tyler M, Liu P, McKenzie D, Suchowerska N.

Over-response of synthetic microDiamond detectors in small radiation fields. Physics in Medicine and Biology. 2014;**59**:5873-5881

[36] Lechner W, Palmans H, Sölkner L, Grochowska P, Georg D. Detector comparison for small field output factor measurements in flattening filter free photon beams. Radiotherapy and Oncology. 2013;**109**:356-360

[37] Scott AJ, Kumar S, Nahum AE, Fenwick JD. Characterizing the influence of detector density on dosimeter response in non-equilibrium small photon fields. Physics in Medicine and Biology. 2012;**57**:4461-4476

[38] Archambault L, Beddar AS, Gingras L, Roy R, Beaulieu L. Measurement accuracy and Cerenkov removal for high performance, high spatial resolution scintillation dosimetry. Medical Physics. 2006;**33**: 128-135

[39] Gagnon J-C et al. Dosimetric performance and array assessment of plastic scintillation detectors for stereotactic radiosurgery quality assurance. Medical Physics. 2012;**39**: 429-436

[40] Morin J et al. A comparative study of small field total scatter factors and dose profiles using plastic scintillation detectors and other stereotactic dosimeters: The case of the CyberKnife. Medical Physics. 2013;**40**:011719

[41] Liu PZY, Suchowerska N, Lambert J, Abolfathi P, McKenzie DR. Plastic scintillation dosimetry: Comparison of three solutions for the Cerenkov challenge. Physics in Medicine and Biology. 2011;**56**: 5805-5821

[42] Devic S. Radiochromic film dosimetry: Past, present, and future. Physica Medica. 2011;**27**:122-134

[43] Bekerat H et al. Improving the energy response of external beam therapy (EBT) GafChromic™ dosimetry films at low energies (≤100 keV). Medical Physics. 2014;**41**:022101

[44] Alnawaf H, Butson MJ, Cheung T, Yu PKN. Scanning orientation and polarization effects for XRQA radiochromic film. Physica Medica. 2010;**26**:216-219

[45] Araki F, Moribe N, Shimonobou T, Yamashita Y. Dosimetric properties of radiophotoluminescent glass rod detector in high-energy photon beams from a linear accelerator and cyber-knife. Medical Physics. 2004;**31**: 1980-1986

[46] Perks J, Gao M, Smith V, Skubic S, Goetsch S. Glass rod detectors for small field, stereotactic radiosurgery dosimetric audit. Medical Physics. 2005; **32**:726-732

[47] Donya H. Pencil-beam fluence evaluation based on Monte Carlo simulations algorithm of high energetic treatment photons. Journal of Medical Signals and Sensors. 2018;**8**:81

[48] Seniwal B, Fonseca TC, Singh R. Monte-Carlo modelling for evaluation of two different calculation algorithms. Brazilian Journal of Radiation Sciences. 2019;**7**(1):1-14

[49] Cunningham JR. Scatter-air ratios. Physics in Medicine and Biology. 1972; **17**(1):42-51

[50] Gupta SK, Cunningham JR. Measurement of tissue-air ratios and scatter functions for large field sizes, for cobalt 60 gamma radiation. The British Journal of Radiology. 1966;**39**(457):7-11

[51] Drouard J, Rosenfeld J-C, Simonian M. Generation of primary and scatter tables for dose computation in high energy photon beams. In:

Proceedings of the 5th ESTRO Meeting on Radiotherapy and Oncology; 1986

[52] ICRU. ICRU Report 23: Measurement of Absorbed Doses in a Phantom Irradiated by a Single Beam of X or Gamma Rays. Bethesda, MD: ICRU; 1973

[53] Kim S, Zhu TC, Palta JR. An equivalent square field formula for determining head scatter factors of rectangular fields. Medical Physics. 1997;**24**(11)

[54] Day MJ. A note on the calculation of dose in X-ray fields. The British Journal of Radiology. 1950;**23**(270): 368-369

[55] Clarkson JR. A note on depth doses in fields of irregular shape. The British Journal of Radiology. 1941;**14**(164): 265-268

[56] Khan FM. The Physics of Radiation Therapy. Baltimore: Williams and Wilkins; 1984

[57] Sterling TD, Perry H, Katz L. Automation of radiation treatment planning—IV. Derivation of a mathematical expression for the per cent depth dose surface of cobalt 60 beams and visualisation of multiple field dose distributions. The British Journal of Radiology. 1964;**37**(439):544-550

[58] Greening JR. Fundamentals of Radiation Dosimetry. Bristol: Adam Hilger; 1981

[59] Mayles P, Nahum A, Rosenwald J-C. Handbook of Radiotherapy Physics: Theory and Practice. New York: Franionization Chambers & Taylor; 2007. p. 1432

[60] Gray LH. The experimental determination by ionization methods of the rate of emission of beta- and gamma-ray energy by radioactive substances. The British Journal of Radiology. 1949;**22**(264):677-697

[61] Ma C, Nahum AE. Bragg-Gray theory and ion chamber dosimetry for photon beams. Physics in Medicine and Biology. 1991;**36**(4):413-428

[62] Spencer LV, Attix FH. A theory of cavity ionization. Radiation Research. 1955;**3**(3):23-54

[63] Nahum AE. Water/air mass stopping power ratios for megavoltage photon and electron beams. Physics in Medicine and Biology. 1978;**23**(1): 24-38

[64] Siebers JV, Keall PJ, Nahum AE, Mohan R. Converting absorbed dose to medium to absorbed dose to water for Monte Carlo based photon beam dose calculations. Physics in Medicine and Biology. 2000;**45**(4):983

[65] Janssens A. Modified energy-deposition model, for the computation of the stopping-power ratio for small cavity sizes. Physical Review A. 1981; **23**(3):1164-1176

[66] Andreo P. Depth-dose and stopping-power data for mono-energetic electron beams. Nuclear Instruments & Methods in Physics Research Section B Beam Interactions with Materials and Atoms. 1990;**51**(2): 107-121

[67] Ahnesjö A, Andreo P, Brahme A. Calculation and application of point spread functions for treatment planning with high energy photon beams. Acta Oncologica. 1987;**26**(1):49-56

[68] Mohan R. Differential pencil beam dose computation model for photons. Medical Physics. 1986;**13**(1):64

[69] Mackie TR. A convolution method of calculating dose for 15-MV X rays. Medical Physics. 1985;**12**(2):188

[70] Eklund K, Ahnesjö A. Fast modelling of spectra and stopping-power ratios using differentiated fluence pencil kernels. Physics in Medicine and Biology. 2008;**53**(16): 4231-4247

[71] Eklund K, Ahnesjö A. Modeling silicon diode dose response factors for small photon fields. Physics in Medicine and Biology. 2010;**55**(24): 7411-7423

[72] Fenwick JD, Kumar S, Scott AJ, Nahum AE. Using cavity theory to describe the dependence on detector density of dosimeter response in non-equilibrium small fields. Physics in Medicine and Biology. 2013;**58**: 2901-2923

[73] Czarnecki D, Zink K. Monte Carlo calculated correction factors for diodes and ion chambers in small photon fields. Physics in Medicine and Biology. 2013; **58**:2431-2444

[74] Czarnecki D, Zink K. Corrigendum: Monte Carlo calculated correction factors for diodes and ion chambers in small photon fields. Physics in Medicine and Biology. 2014;**59**:791-794

[75] Francescon P, Cora S, Satariano N. Calculation of for several small detectors and for two linear accelerators using Monte Carlo simulations. Medical Physics. 2011;**38**:6513-6527

[76] Francescon P, Kilby W, Satariano N, Cora S. Monte Carlo simulated correction factors for machine specific reference field dose calibration and output factor measurement using fixed and iris collimators on the CyberKnife system. Physics in Medicine and Biology. 2012;**57**:3741-3758

[77] Sanchez-Doblado F et al. Ionization chamber dosimetry of small photon fields: A Monte Carlo study on stopping-power ratios for radiosurgery and IMRT beams. Physics in Medicine and Biology. 2003;**48**:2081-2099

[78] Sharma SC, Ott JT, Williams JB, Dickow D. Commissioning and acceptance testing of a CyberKnife linear accelerator. Journal of Applied Clinical Medical Physics. 2007;**8**:119-125

[79] British Institute of Radiology. Central Axis Depth Dose Data for Use in Radiotherapy Departments: 1996, BJR Supplement 25. London: BIR; 1996

[80] Sauer OA, Wilbert J. Measurement of output factors for small photon beams. Medical Physics. 2007;**34**: 1983-1988

[81] Alfonso R et al. A new formalism for reference dosimetry of small and nonstandard fields. Medical Physics. 2008;**35**:5179-5186

[82] Thomas SD, MacKenzie M, Rogers DWO, Fallone BG. A Monte Carlo derived TG-51 equivalent calibration for helical tomotherapy. Medical Physics. 2005;**32**:1346-1353

[83] Langen KM et al. QA for helical tomotherapy: Report of the AAPM task group 148. Medical Physics. 2010;**37**: 4817-4853

[84] Zeverino M, Agostinelli S, Pupillo F, Taccini G. Determination of the correction factors for different ionization chambers used for the calibration of the helical tomotherapy static beam. Radiotherapy and Oncology. 2011;**100**:424-428

[85] Sauer OA. Determination of the quality index (Q) for photon beams at arbitrary field sizes. Medical Physics. 2009;**36**:4168-4172

[86] Andreo P. On the beam quality specification of high-energy photons for radiotherapy dosimetry. Medical Physics. 2000;**27**:434-440

[87] Xiong G, Rogers DWO. Relationship between %dd(10)x and stopping-power ratios for flattening filter free accelerators: A Monte Carlo study. Medical Physics. 2008;**35**:2104-2109

[88] Palmans H, National Physical Laboratory. Personal Communication; 2015

[89] Dalaryd M, Knöös T, Ceberg C. Combining tissue-phantom ratios to provide a beam-quality specifier for flattening filter free photon beams. Medical Physics. 2014;**41**:111716

[90] Palmans H. Determination of the beam quality index of high-energy photon beams under nonstandard reference conditions. Medical Physics. 2012;**39**:5513-5519

[91] Podgorsak EB. External photon beams: Physical aspects. In: Radiation Oncology Physics: A Handbook.

[92] Verhaegen F, Das IJ, Palmans H. Monte Carlo dosimetry study of a 6 MV stereotactic radiosurgery unit. Physics in Medicine & Biology. 1998;**43**(10): 2755

[93] Ding GX, Duggan DM, Coffey CW. Comment on "Testing of the analytical anisotropic algorithm for photon dose calculation" [Med. Phys. 33, 4130-4148 (2006)]. Medical Physics. 2007;**34**(8): 3414

[94] Kijewski PK, Bjärngard BE, Petti PL. Monte Carlo calculations of scatter dose for small field sizes in a 60Co beam. Medical Physics. 1986;**13**(1):74-77

[95] Ding GX, Duggan DM, Coffey CW. Commissioning stereotactic radiosurgery beams using both experimental and theoretical methods. Physics in Medicine & Biology. 2006; **51**(10):2549

[96] Ding GX. Dose discrepancies between Monte Carlo calculations and measurements in the buildup region for a high-energy photon beam. Medical Physics. 2002;**29**(11): 2459-2463

[97] Ding GX. Using Monte Carlo simulations to commission photon beam output factors—A feasibility study. Physics in Medicine & Biology. 2003; **48**(23):3865

[98] Ahnesjö A. Collimator scatter in photon therapy beams. Medical Physics. 1995;**22**(3):267-278

[99] Jones AO, Das IJ, Jones FL Jr. A Monte Carlo study of IMRT beamlets in inhomogeneous media. Medical Physics. 2003;**30**(3):296-300

[100] Jones AO, Das IJ. Comparison of inhomogeneity correction algorithms in small photon fields. Medical Physics. 2005;**32**(3):766-776

[101] Saitoh H, Fujisaki T, Sakai R, Kunieda E. Dose distribution of narrow beam irradiation for small lung tumor. International Journal of Radiation Oncology Biology Physics. 2002;**53**(5): 1380-1387

[102] Al-Hallaq HA, Reft CS, Roeske JC. The dosimetric effects of tissue heterogeneities in intensity-modulated radiation therapy (IMRT) of the head and neck. Physics in Medicine & Biology. 2006;**51**(5):1145

[103] Paelinck L, Reynaert N, Thierens H, De Neve W, De Wagter C. Experimental verification of lung dose with radiochromic film: Comparison with Monte Carlo simulations and commercially available treatment planning systems. Physics in Medicine & Biology. 2005;**50**(9):2055

[104] Krieger T, Sauer OA. Monte Carlo-versus pencil-beam−/collapsed-cone-dose calculation in a heterogeneous multi-layer phantom. Physics in Medicine & Biology. 2005;**50**(5):859

[105] Chetty IJ, Charland PM, Tyagi N, McShan DL, Fraass BA, Bielajew AF. Photon beam relative dose validation of the DPM Monte Carlo code in lung-equivalent media. Medical Physics. 2003;**30**(4):563-573

[106] Rogers DWO, Kawrakow I, Seuntjens JP, Walters BRB, Mainegra-Hing E. NRC user codes for EGSnrc. NRCC Report PIRS-702 (Rev. B). 2003

[107] GEANT Collaboration, Agostinelli S. GEANT4—A simulation toolkit. Nuclear Instruments and Methods A. 2003;**506**(25)

[108] MCNP—A General Monte Carlo. N-Particle Transport Code. Vol. I: Overview and Theory. Los Alamos, NM: Los Alamos National Laboratory; 2003. LA-UR-03-1987

[109] Heydarian M, Hoban PW, Beddoe AH. A comparison of dosimetry techniques in stereotactic radiosurgery. Physics in Medicine & Biology. 1996;**41**(1):93

[110] Scielzo G, Grillo FR, Schwarz M, Rivolta A, Brunelli B, Surridge M, et al. The Monte Carlo method and parallel estimation in the drawing up of radiosurgery treatment plans. La Radiologia Medica. 1998;**95**(6):647-655

[111] De Vlamynck K, Palmans H, Verhaegen F, De Wagter C, De Neve W, Thierens H. Dose measurements compared with Monte Carlo simulations of narrow 6 MV multileaf collimator shaped photon beams. Medical Physics. 1999;**26**(9):1874-1882

[112] Cheung YC, Yu KN, Ho RTK, Yu CP. Stereotactic dose planning system used in Leksell gamma knife model-B: EGS4 Monte Carlo versus GafChromic films MD-55. Applied Radiation and Isotopes. 2000;**53**(3):427-430

[113] Westermark M, Arndt J, Nilsson B, Brahme A. Comparative dosimetry in narrow high-energy photon beams. Physics in Medicine & Biology. 2000;**45**(3):685

[114] Deng J, Ma CM, Hai J, Nath R. Commissioning 6 MV photon beams of a stereotactic radiosurgery system for Monte Carlo treatment planning. Medical Physics. 2003;**30**(12):3124-3134

[115] Paskalev KA, Seuntjens JP, Patrocinio HJ, Podgorsak EB. Physical aspects of dynamic stereotactic radiosurgery with very small photon beams (1.5 and 3 mm in diameter). Medical Physics. 2003;**30**(2):111-118

[116] Tsougos I, Theodorou K, Bazioglou M, Stathakis S. Kappas C. a comparison of Monte Carlo simulation with experimental dosimetric techniques for a 6 MV stereotactic radiotherapy unit. Journal of BUON. 2004;**9**:451-564

[117] Francescon P, Cora S, Cavedon C. Total scatter factors of small beams: A multidetector and Monte Carlo study. Medical Physics. 2008;**35**(2):504-513

[118] Heydarian M, Asnaashari K, Allahverdi M, Jaffray DA. Dosimetric evaluation of a dedicated stereotactic linear accelerator using measurement and Monte Carlo simulation. Medical Physics. 2008;**35**(9):3943-3954

[119] Cranmer-Sargison G, Charles PH, Trapp JV, Thwaites DI. A methodological approach to reporting corrected small field relative outputs. Radiotherapy and Oncology. 2013;**109**(3):350-355

[120] Charles PH, Cranmer-Sargison G, Thwaites DI, Crowe SB, Kairn T, Knight RT, et al. A practical and theoretical definition of very small field size for radiotherapy output factor measurements. Medical Physics. 2014;**41**(4):041707

[121] Francescon P, Kilby W, Satariano N, Orlandi C, Elshamndy SK. The impact of inter-unit variations on small field dosimetry correction factors, with application to the CyberKnife system. Physics in Medicine and Biology. 2018

[122] Casar B, Gershkevitsh E, Mendez I, Jurković S, Huq MS. A novel method for the determination of field output factors and output correction factors for small static fields for six diodes and a microdiamond detector in megavoltage photon beams. Medical Physics. 2019;**46**(2):944-963

[123] Freud N, Letang JM, Mary C, Boudou C, Ferrero C, Elleaume H, et al. A hybrid approach for fast simulation of dose deposition in stereotactic synchrotron radiotherapy. IEEE Transactions on Nuclear Science. 2008;**55**(3):1008-1017

[124] Freud N, Letang JM, Mary C, Boudou C, Ferrero C, Elleaume H, et al. Fast dose calculation for stereotactic synchrotron radiotherapy. In: 2007 29th Annual International Conference of the IEEE Engineering in Medicine and Biology Society. IEEE; 2007. pp. 3914-3917

[125] Chetty IJ, Curran B, Cygler JE, DeMarco JJ, Ezzell G, Faddegon BA, et al. Report of the AAPM Task Group No. 105: Issues associated with clinical implementation of Monte Carlo-based photon and electron external beam treatment planning. Medical Physics. 2007;**34**(12):4818-4853

[126] Jang SY, Liu HH, Mohan R. Underestimation of low-dose radiation in treatment planning of intensity-modulated radiotherapy. International Journal of Radiation Oncology Biology Physics. 2008;**71**(5):1537-1546

[127] Petti PL, Chuang CF, Smith V, Larson DA. Peripheral doses in CyberKnife radiosurgery. Medical Physics. 2006;**33**(6 Part 1):1770-1779

[128] Chuang CF, Larson DA, Zytkovicz A, Smith V, Petti PL. Peripheral dose measurement for CyberKnife radiosurgery with upgraded linac shielding. Medical Physics. 2008;**35**(4):1494-1496

[129] Di Betta E, Fariselli L, Bergantin A, Locatelli F, Del Vecchio A, Broggi S, et al. Evaluation of the peripheral dose in stereotactic radiotherapy and radiosurgery treatments. Medical Physics. 2010;**37**(7 Part 1):3587-3594